Chapter 2

PHOTOCHEMISTRY OF $B_{12}(OR)_{12}$

Parts of the work discussed in this chapter was published in Axtell, J. C.; Messina, M. S.; Liu, J.-Y.; Galaktionova, D.; Schwan, J.; Porter, T. M.; Savage, M. D.; Wixtrom, A. I.; Rheingold, A. L.; Kubiak, C. P.; et al. Photooxidative Generation of Dodecaborate-Based Weakly Coordinating Anions. *Inorg. Chem.* **2019**, *58* (16), 10516–10526. The paper can be found in its entirety in Appendix A.

Chapter 2 summarizes my contributions to a broad collaborative effort exploring the photochemistry of $B_{12}(OR)_{12}$ *clusters. Much of the results presented here have not previously been published, and the discussion is at times speculative. That said, our observations helped direct mechanistic and computation work reported in the paper mentioned above and could assist in guiding future research.*

The hypercloso-$B_{12}(OR)_{12}$ *clusters* $B_{12}(OC_6F_5)_{12}$ (**F_{60}^0**), $B_{12}(4\text{-}CF_3\text{-}C_6H_4)_{12}$ (**F_{36}^0**), $B_{12}(3,5\text{-}(CF_3)_2\text{-}C_6H_3)_{12}$ (**F_{72}^0**) *and* $B_{12}(3,5\text{-}(CF_3)_2\text{-}C_6F_3)_{12}$ (**F_{84}^0**) *form small amounts of anionic* $[B_{12}]^{1-}$ *in many solvents.* $[B_{12}]^{1-}$ *show fluorescence centered at 600 nm. This complicates photophysical characterization of* B_{12}^0*, as the emission spectrum is often dominated by* $[B_{12}]^{1-}$*. We sought to understand what causes formation of* $[B_{12}]^{1-}$ *and find ways to eliminate its contribution to the emission spectra of* B_{12}^0*. Some instances of* $[B_{12}]^{1-}$ *formation can be explained by direct solvent oxidation or photooxidation, however, our results suggest that complex solvent-cluster interactions may also play a role. Furthermore, we found that* $[B_{12}]^{1-}$ *disproportionate in the presence of trifluoracetic acid, and at cryogenic temperatures in 2-methyltetrahydrofuran. Our work culminated in collection of emission data for* **F_{36}^0**, **F_{60}^0**, *and* **F_{72}^0** *at 77 K in 10:1 perfluorotoluene/perfluoro-methylcyclohexane glass.*

2.1 Background

Icosahedral dodecaborate clusters have been known since the late 1950s, when Lipscomb and co-workers first synthesized *closo*-$[B_{12}H_{12}]^{2-}$.[2–9] These closed-shell clusters display no visible absorption bands due to the large energy gap between the highest occupied molecular orbital (HOMO) and lowest unoccupied molecular orbital (LUMO). Over the past few decades, a range of hypoelectronic perfunctionalized dodecaborate clusters have been isolated in oxidized *hypocloso*-$[B_{12}]^{1-}$ and *hypercloso*-B_{12}^{0} states (B_{12} denotes a generic perfunctionalized dodecaborate cluster). Early examples include *hypocloso*-$[B_{12}Me_{12}]^{1-}$ (Me = CH_3),[10] *hypocloso*-$[B_{12}X_{12}]^{1-}$ (X = F, Cl, Br, I),[11–13] *hypocloso*-$[B_{12}(OH)_{12}]^{1-}$,[14] *hypocloso*-$[B_{12}(OBz)_{12}]^{1-}$ and *hypercloso*-$B_{12}(OBz)_{12}$ (Bz = $CH_2C_6H_5$).[15] These oxidized dodecaborate clusters undergo structural distortions breaking the fourfold degeneracy of the *closo*-$[B_{12}]^{2-}$ HOMO, which helps stabilize the hypoelectronic cluster core. They also display rich visible absorption spectra due to excitations between lower lying molecular orbitals and the HOMO vacancies resulting from oxidation.

Spokoyny and co-workers first reported the exceptional photooxidizing ability of perfunctionalized dodecaborate clusters in 2016 (Messina et al. 2016).[16] They realized that that *hypocloso*-$B_{12}(OBz)_{12}$ could photoinitiate polymerization of electron-rich styrenes, such as 4-methoxy-styrene (**2a**). Following these findings, they decided to explore whether more oxidizing $B_{12}(OR)_{12}$ clusters could initiate polymerization of less-accessible substrates. Indeed, they found that the perfluorophenyl derivative *hypercloso*-$B_{12}(OCH_2C_6F_5)_{12}$ ($\mathbf{F_{60}}^{0}$; nomenclature based on the number of fluorine atoms) could initiate polymerization of a range of styrenes, including both electron-rich and electron-poor variants (Table 2.1, **2b**-**2i**). Hoping to expand the reactivity to even more challenging monomers, they turned their attention to isobutylene. By ^{1}H- and ^{13}C-NMR, they showed that after 4 hours of 450 nm illumination a highly branched polymer had formed in a 2 mM solution of $\mathbf{F_{60}}^0$ under 1–4 psi isobutylene. A ^{1}H-NMR spectrum of the highly branched poly(isobutylene) product is shown in Figure 2.1. The ability to photoinitiate isobutylene polymerization in a metal-free system is noteworthy, as such reactivity had previously been reserved for transition metal photoinitiators. Time-dependent density functional theory (TD-DFT) was used explain the reactivity by comparing the LUMO energy of *hypercloso*-$B_{12}(OBz)_{12}$ and $\mathbf{F_{60}}^0$ with the HOMO energy of the styrene monomers. Attempts to use TD-DFT to examine the orbitals involved in photoexcitation indicated that the lowest energy electronic transition occur between a low-lying orbital (HOMO-27 in $\mathbf{F_{60}}^0$ and HOMO-15 in $B_{12}(OBz)_{12}$) and the LUMO. Photophysical characterization was performed using both steady-state fluorescence measurements and fluorescence decay measurements. Steady-state measurements with $\mathbf{F_{60}}^0$ in dichloromethane, benzene, trifluoromethylbenzene and 1,2-difluorobenzene showed a fluorescence maximum around 600 nm with highly solvent dependent intensity. $\mathbf{F_{60}}^0$ in dichloromethane showed near-zero fluorescence, while $\mathbf{F_{60}}^0$ in 1,2-difluorobenzene showed medium-to-intense fluorescence. Decay measurements using 355 nm laser excitation gave a lifetime of a few hundreds of picoseconds at 600 nm in acetonitrile and 1,2-dichlorobenzene. Based on the emission data, the excited-state reduction potential of $\mathbf{F_{60}}^0$ was estimated to around 3 V (vs the standard calomel electrode).[16]

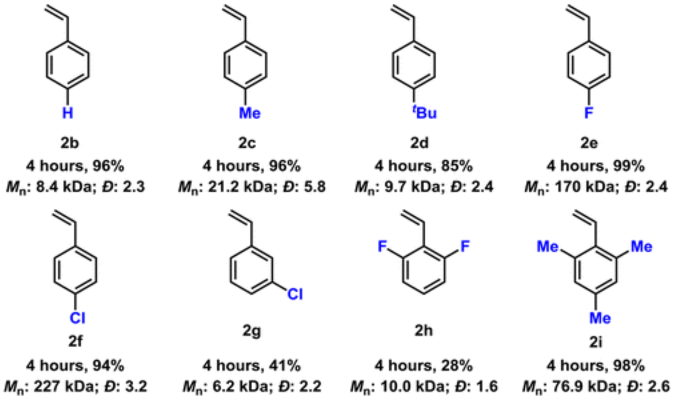

Table 2.1. Monomers polymerized by $\mathbf{F_{60}}^{\mathbf{0}}$ (0.1 mol%) in dichloromethane. Yield, molecular weight (M_n) and dispersity (Đ) shown for each monomer. Reprinted with permission from Messina, M. S.; Axtell, J. C.; Wang, Y.; Chong, P.; Wixtrom, A. I.; Kirlikovali, K. O.; Upton, B. M.; Hunter, B. M.; Shafaat, O. S.; Khan, S. I.; et al. Visible-Light-Induced Olefin Activation Using 3D Aromatic Boron-Rich Cluster Photooxidants. *Journal of the American Chemical Society* **2016**, *138* (22), 6952–6955. Copyright (2016) American Chemical Society.

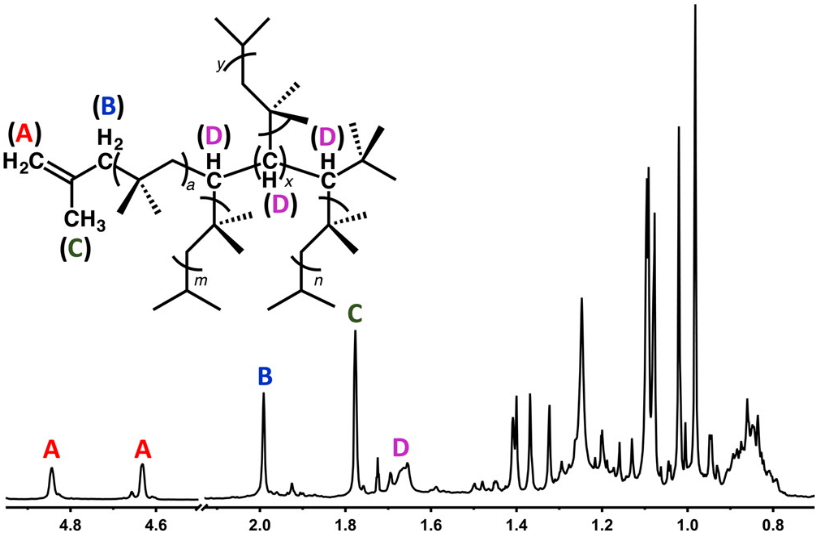

Figure 2.1. ^{1}H-NMR of poly(isobuylene) produced by irradiation of $\mathbf{F_{60}}^0$ with a 450 nm light-emitting diode (LED) under 4 psi isobutylene. Label A indicates protons of the olefinic chain end; B/C, allylic protons of the chain end; D, methine protons. Reprinted with permission from Messina, M. S.; Axtell, J. C.; Wang, Y.; Chong, P.; Wixtrom, A. I.; Kirlikovali, K. O.; Upton, B. M.; Hunter, B. M.; Shafaat, O. S.; Khan, S. I.; et al. Visible-Light-Induced Olefin Activation Using 3D Aromatic Boron-Rich Cluster Photooxidants. *Journal of the American Chemical Society* **2016**, *138* (22), 6952–6955. Copyright (2016) American Chemical Society

2.2 Preliminary Photophysical Studies

The original goal of the work presented in this Chapter was to improve on the results reported in the initial $B_{12}(OR)_{12}$ photooxidation paper (Messina et al. 2016).[16] We knew from our records that the samples used for the published data set had been changing color during collection. At the time, the hypothesis was that the relatively short lifetimes and inconsistent fluorescence spectra resulted from unwanted side reactions caused by trace impurities. We believed these issues could be circumvented by using more stringent sample preparation and handling methods, and that this would lead to lifetimes more consistent with a diffusion controlled photooxidation mechanism.

We started by attempting to collect reproducible emission data and lifetime measurements. In addition to $\mathbf{F_{60}}^0$, the study was expanded to *hypercloso*-$B_{12}(4\text{-}CF_3\text{-}C_6H_4)_{12}$ ($\mathbf{F_{36}}^0$), *hypercloso*-$B_{12}(3,5\text{-}(CF_3)_2\text{-}C_6H_3)_{12}$ ($\mathbf{F_{76}}^0$) and *hypercloso*-$B_{12}(3,5\text{-}(CF_3)_2\text{-}C_6F_3)_{12}$ ($\mathbf{F_{84}}^0$). Based on records from previous researchers we expected that $\mathbf{F_{76}}^0$ and, in particular, $\mathbf{F_{84}}^0$ would be significantly stronger emitters than $\mathbf{F_{60}}^0$. Hoping to combine the strongest emitter with the best solvent, we prepared samples of $\mathbf{F_{84}}^0$ in 1,2-difluorobenzene. Immediately, it became clear that $\mathbf{F_{84}}^0$ was not stable under these conditions, as the sample solution rapidly changed color from yellow to purple. Preliminary fluorescence measurements were, as expected, similar to the published spectra. Hoping to improve the data, we prepared samples of $\mathbf{F_{84}}^0$ under low-light conditions using dry and air-free 1,2-difluorobenzene. No significant color shifts were observed by eye when the samples were prepared under low-light conditions. In direct contrast to our expectations, preliminary fluorescence intensities for these samples were significantly lower than what we had observed for samples prepared under ambient conditions. However, samples turned purple during data collection and the fluorescence intensity rapidly increased as more scans were averaged. The low-light experiments were repeated for $\mathbf{F_{60}}^0$ and $\mathbf{F_{72}}^0$, again displaying significantly reduced fluorescence compared to samples prepared under ambient lighting. Notably, comparison of the three clusters indicated that increased fluorine content was correlated to both stronger preference for the purple state and more intense fluorescence. Reproducible spectra could not be collected under the given conditions and we were unable to obtain excitation spectra that matched the absorption spectra of the neutral clusters. We wonder what the nature of the purple species was and whether it could be responsible for the observed fluorescence spectra.

Comparison of the UV-visible absorption spectrum of the purple $\mathbf{F_{60}}$ samples showed an uncanny resemblance to the published spectrum of $[\mathbf{F_{60}}]^{1-}$. However, the extinction coefficients we observed were several times higher than what had previously been reported for $[\mathbf{F_{60}}]^{1-}$.[16] We hypothesized that the purple species' was the result of B_{12}^0 photoreduction to $[B_{12}]^{1-}$ and that the reported extinction coefficient for $[\mathbf{F_{60}}]^{1-}$ was incorrect. Although this explanation was attractive, we felt photoreduction alone might not be sufficient to rationalize our observations. Our primary concern was that in 1,2-difluorobenzene a weak 525 nm band immediately appeared after mixing, even in the dark. This behavior persisted regardless of solvent manufacturer, and whether the solvent had been dried and degassed. These observations lead to a competing hypothesis: the purple species is the result of cluster-solvent interactions, possibly involving solvent and concentration-dependent cluster aggregation.

2.3 Electrochemical Characterization and the $[B_{12}]^{1-}$ Monoanion

Cyclic voltammograms of $\mathbf{F_{60}}$ and $\mathbf{F_{72}}$ collected at 100 mV/s in 0.2 M $TBAPF_6$ (tetrabutylammonium hexafluorophosphate) dichloromethane electrolyte are shown in Figure

2.2 A-B. Two waves are observed for both clusters, representing the $[B_{12}]^{1-/2-}$ and $[B_{12}]^{0/1-}$ couples. The influence of scan rate (ν) on the peak potential (i_p) was explored to assess the reversibility of the redox events. The electrochemical reversibility is confirmed by the linear relationships between i_p and $(\nu)^{1/2}$, shown in Figure 2.3 (**F**$_{60}$) and 2.4 (**F**$_{72}$) along with individual cyclic voltammograms collected for each redox couple. Table 2.2 summarizes the redox potentials measured for **F**$_{60}$ and **F**$_{72}$.

Table 2.2. Redox potentials derived from a cyclic voltammograms collected at 100 mV/s in 0.2 M TBAPF$_6$ dichloromethane solution. E_p^{ox} and E_p^{red} are the oxidative and reductive peak potentials. $E_{1/2}$ is the mean of the peak potentials. All potentials are referenced to the ferrocene-ferrocenium couple.

	$[\mathbf{F}_{60}]^{1-/2-}$	$[\mathbf{F}_{60}]^{0/1-}$	$[\mathbf{F}_{72}]^{1-/2-}$	$[\mathbf{F}_{72}]^{0/1-}$
E_p^{ox} (V)	-0.124	0.593	0.182	0.922
E_p^{red} (V)	-0.196	0.515	0.097	0.776
$E_{1/2}$ (V)	-0.160	0.554	0.140	0.844

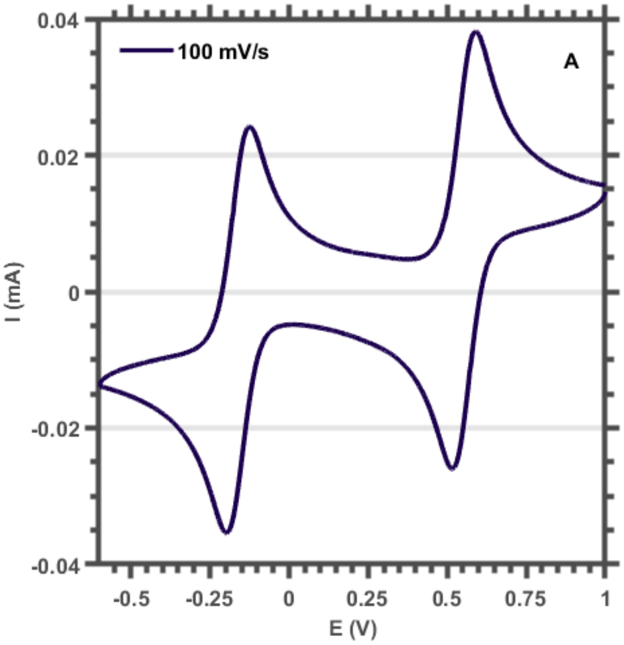

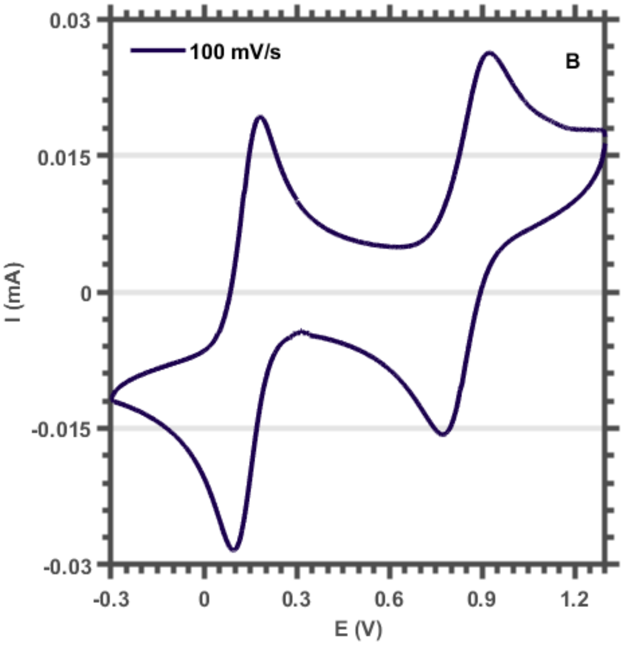

Figure 2.2. Cyclic voltammograms collected for (A) $\mathbf{F_{60}}$ and (B) $\mathbf{F_{72}}$ at 100 mV/s in 0.2 M $TBAPF_6$ dichloromethane electrolyte.

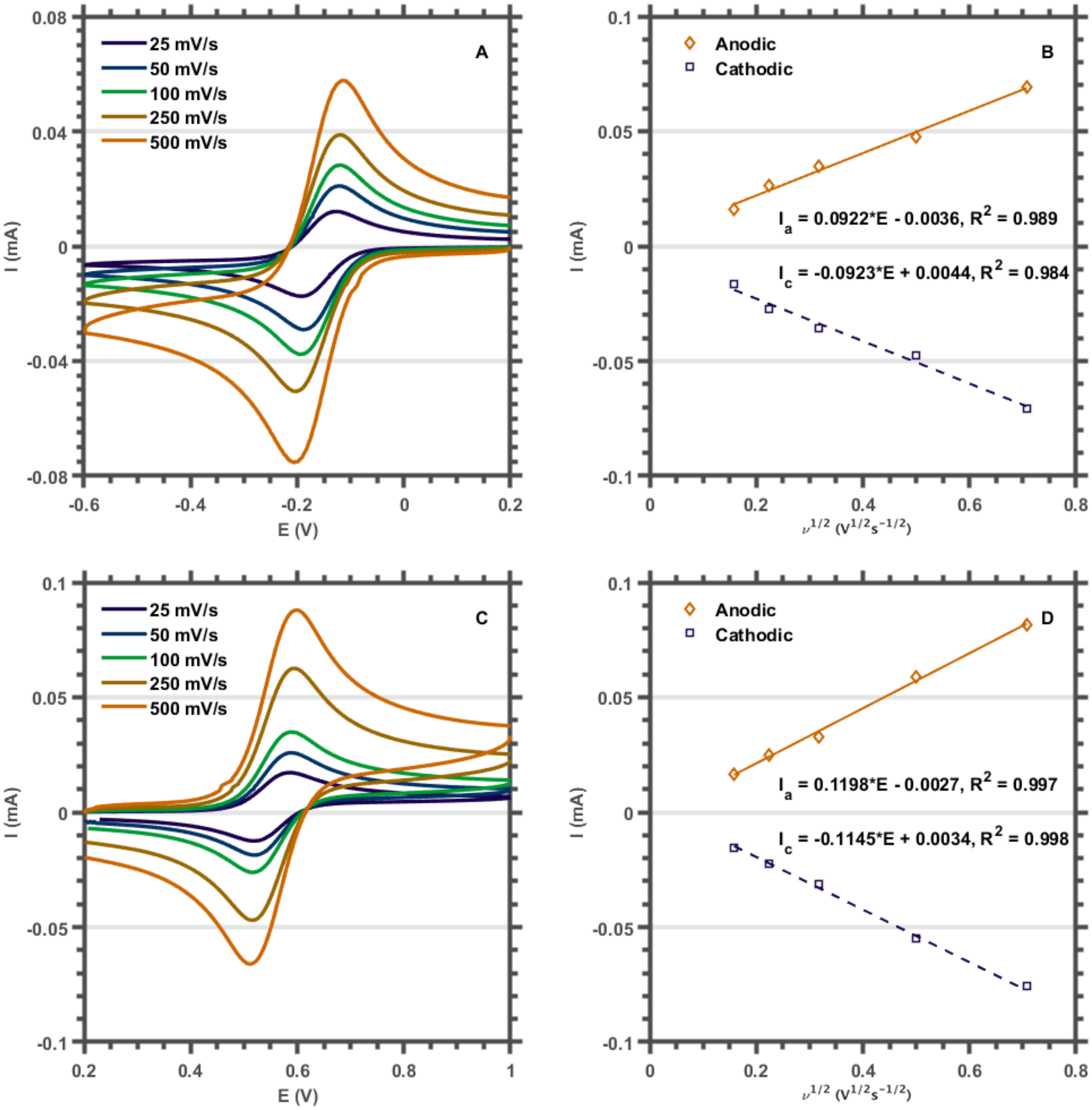

Figure 2.3. Scan rate dependence of 2.5 mM **F$_{60}$** in 0.2 M TBAPF$_6$/dichloromethane. i_a and i_c are the anodic and cathodic peak potentials. ν is the scan rate in V/s. (A) [**F$_{60}$**]$^{1-/2-}$ cyclic voltammograms, (B) i_p([**F$_{60}$**]$^{1-/2-}$) as a function of $(\nu)^{1/2}$, (C) [**F$_{60}$**]$^{1-/2-}$ cyclic voltammograms, (D) i_p([**F$_{60}$**]$^{0/1-}$) as a function of $(\nu)^{1/2}$.

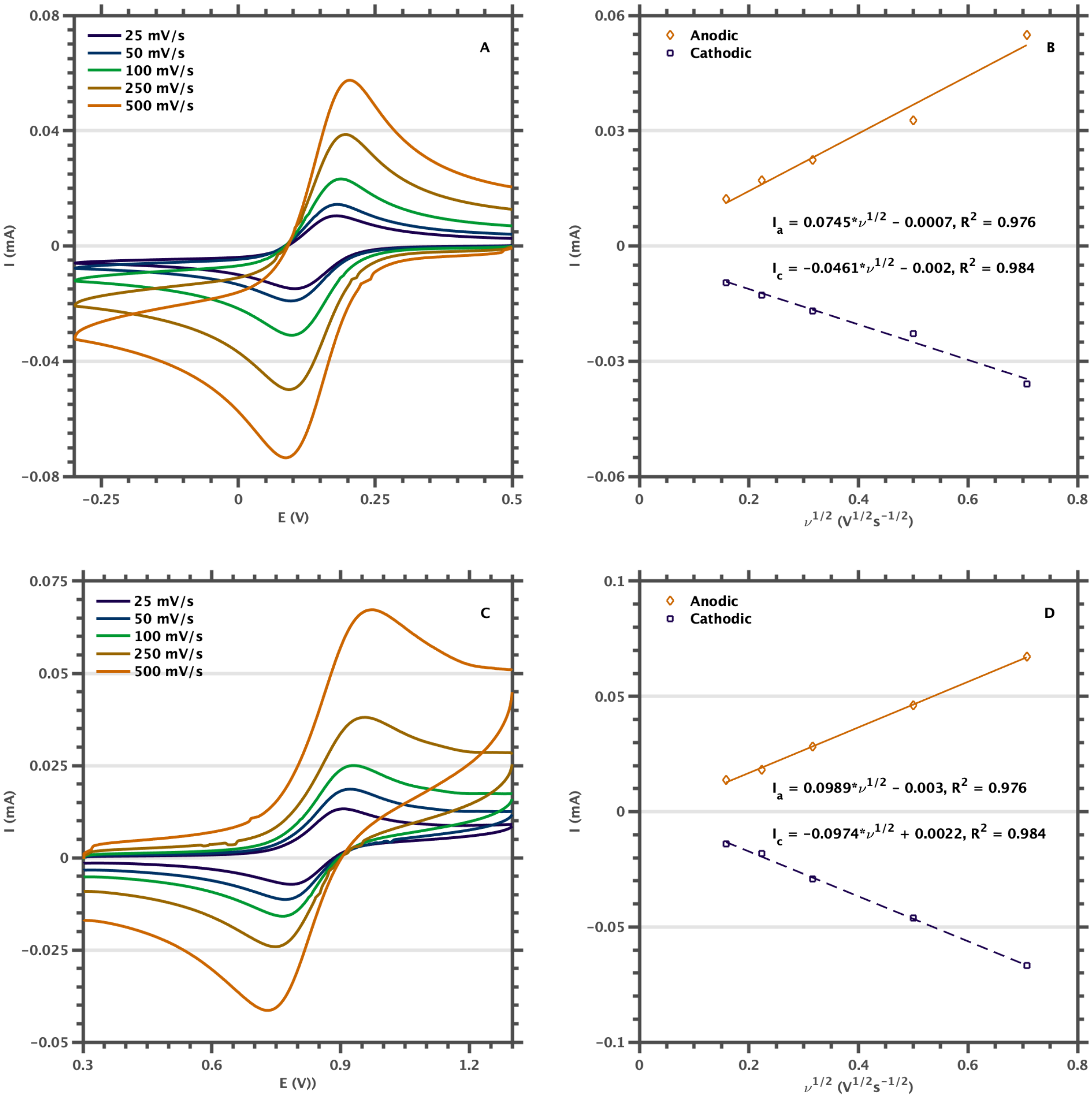

Figure 2.4. Scan rate dependence of ~2.3 mM $\mathbf{F_{72}}$ in 0.2 M TBAPF$_6$/dichloromethane. i_a and i_c are the anodic and cathodic peak potentials. ν is the scan rate in V/s. (A) $[\mathbf{F_{72}}]^{1-/2-}$ cyclic voltammograms, (B) $i_p([\mathbf{F_{72}}]^{1-/2-})$ as a function of $(\nu)^{1/2}$, (C) $[\mathbf{F_{72}}]^{1-/2-}$ cyclic voltammograms, (D) $i_p([\mathbf{F_{72}}]^{0/1-})$ as a function of $(\nu)^{1/2}$.

Following electrochemical characterization, we used spectroelectrochemistry to show that the published extinction coefficient of the $[\mathbf{F_{60}}]^{1-}$ 525 nm band had been significantly underestimated, and that the true spectrum was in good agreement with the purple species we had observed during our preliminary work. Spectroelectrochemical data collected for $\mathbf{F_{60}}$ in benzonitrile is shown in Figure 2.5 A-B, while Figure 2.6 A-C shows data collected in dichloromethane. In benzonitrile, it proved challenging to achieve complete conversion to $[\mathbf{F_{60}}]^{2-}$ but we were able to successfully achieve near-complete conversion to $\mathbf{F_{60}}^{0}$ and $[\mathbf{F_{60}}]^{1-}$. Significant non-Coulombic currents were passed, indicating that side reactions may have been occurring. In dichloromethane, $\mathbf{F_{60}}$ was taken all the way from $[\mathbf{F_{60}}]^{2-}$ to $\mathbf{F_{60}}^{0}$. This data led us to conclude that $[\mathbf{F_{60}}]^{1-}$ has a visible absorption band at 525 nm with approximately half the extinction coefficient of the 455 nm band of $\mathbf{F_{60}}^{0}$. Later extinction coefficient measurements based on chemically isolated [TBA][$\mathbf{F_{60}}$] and [TBA][$\mathbf{F_{72}}$] further validate these results, finding a strong ~455 nm band for the neutral B_{12} clusters ($\varepsilon_{455nm} \approx 25{,}000\ M^{-1}cm^{-1}$) and a slightly weaker ~525 nm band for the monoanionic $[B_{12}]^{1-}$ clusters ($\varepsilon_{525nm} \approx 13{,}000\ M^{-1}cm^{-1}$). These observations strongly support that the 525 nm band stems from formation of monoanionic $[B_{12}]^{1-}$ cluster.

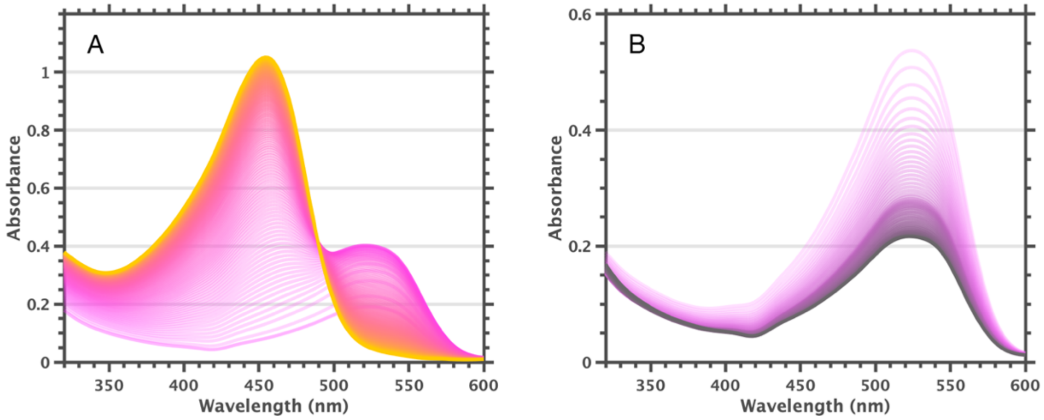

Figure 2.5. Electrochemically derived spectra of $\mathbf{F_{60}}$ collected in 0.1 M TBAPF$_6$/Benzonitrile. (a) $[\mathbf{F_{60}}]^{2-/1-}$ mixture oxidized to $[\mathbf{F_{60}}]^{1-}$, then $\mathbf{F_{60}}^{0}$. (b) $[\mathbf{F_{60}}]^{1-}$ reduced to a $[\mathbf{F_{60}}]^{2-/1-}$ mixture.

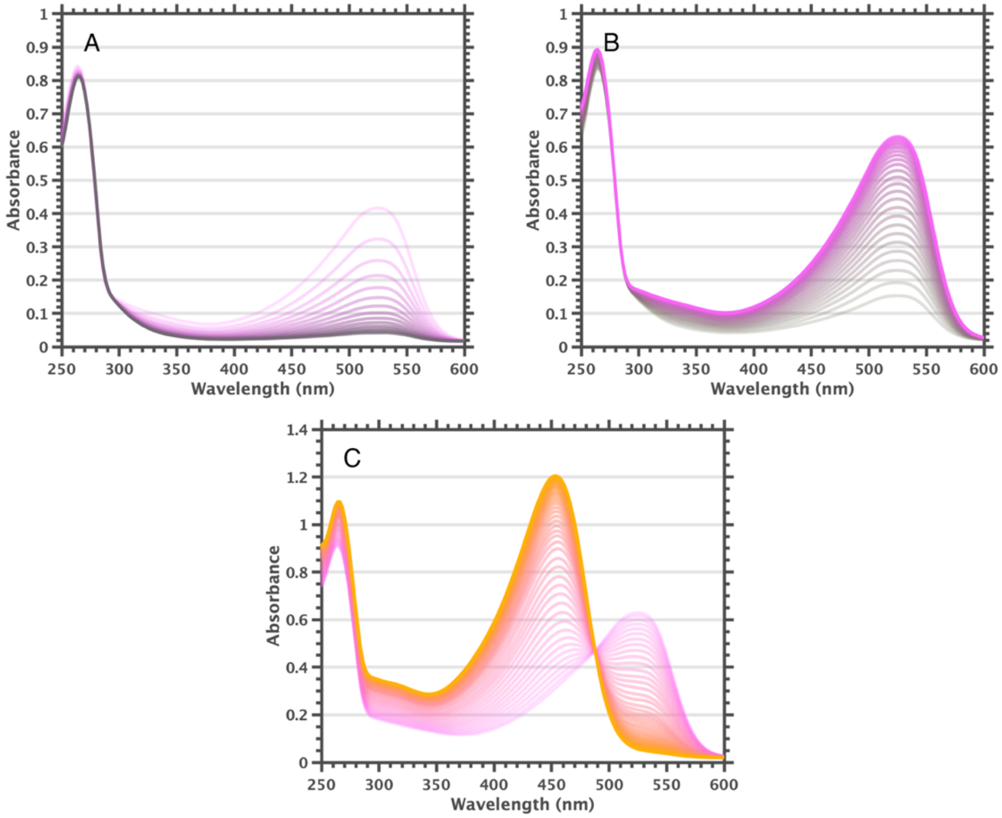

Figure 2.6. Electrochemically derived spectra of $\mathbf{F_{60}}$ collected in 0.1 M TBAPF$_6$/dichloromethane. (a) $[\mathbf{F_{60}}]^{1-}$ reduced to $[\mathbf{F_{60}}]^{2-}$. (b) $[\mathbf{F_{60}}]^{2-}$ oxidized to $[\mathbf{F_{60}}]^{1-}$. (c) $[\mathbf{F_{60}}]^{1-}$ oxidized to $\mathbf{F_{60}}^{0}$.

2.4 Interactions with Haloarenes

We now wanted to understand what caused formation $[B_{12}]^{1-}$. As our initial work indicated that conversion to $[B_{12}]^{1-}$ was most strongly favored in 1,2-difluorobezene, we wondered if other halogenated aromatic solvents would also favor $[B_{12}]^{1-}$ and whether concentration-dependent aggregation mechanisms where involved. To explore aggregation, we performed Beer's law measurements of $\mathbf{F_{60}}^{0}$ in benzene, toluene, chlorobenzene and 1,2-dichlorobenzene (Figure 2.7 A-D). Aggregation-induced spectral changes are unlikely if absorption is linearly dependent on concentration. The 455 nm absorption band showed good agreement with Beers' law (Figure 2.7 E-H) giving no indication of concentration-induced aggregation, although a small 525 nm shoulder was seen in all solvents except chlorobenzene.

A follow-up experiment was performed where a concentrated $\mathbf{F_{60}}^{0}$ solution in dry and degassed 1,2-dichlorobenzene was slowly added to neat solvent. The stock solution had a bright yellow color implying little contribution from the 525 nm band. UV-visible spectra collected after each addition are shown in Figure 2.8. Remarkably, $[\mathbf{F_{60}}]^{1-}$ dominates the spectrum throughout the concentration series indicating that $\mathbf{F_{60}}^{0}$ is kinetically inert at higher concentrations but readily converts to $[\mathbf{F_{60}}]^{1-}$ when diluted. This could indicate that, while aggregation does not shift the visible absorption bands, kinetically inert aggregated forms of $\mathbf{F_{60}}^{0}$ may be present at elevated concentrations.

To further test the cluster-solvent interaction hypothesis, we wanted to find a solvent where $[\mathbf{F_{60}}]^{1-}$ was strongly favored. The results from the Beer's law study indicated that a higher degree of halogenation led to a more pronounced 525 nm shoulder. To test this, we added

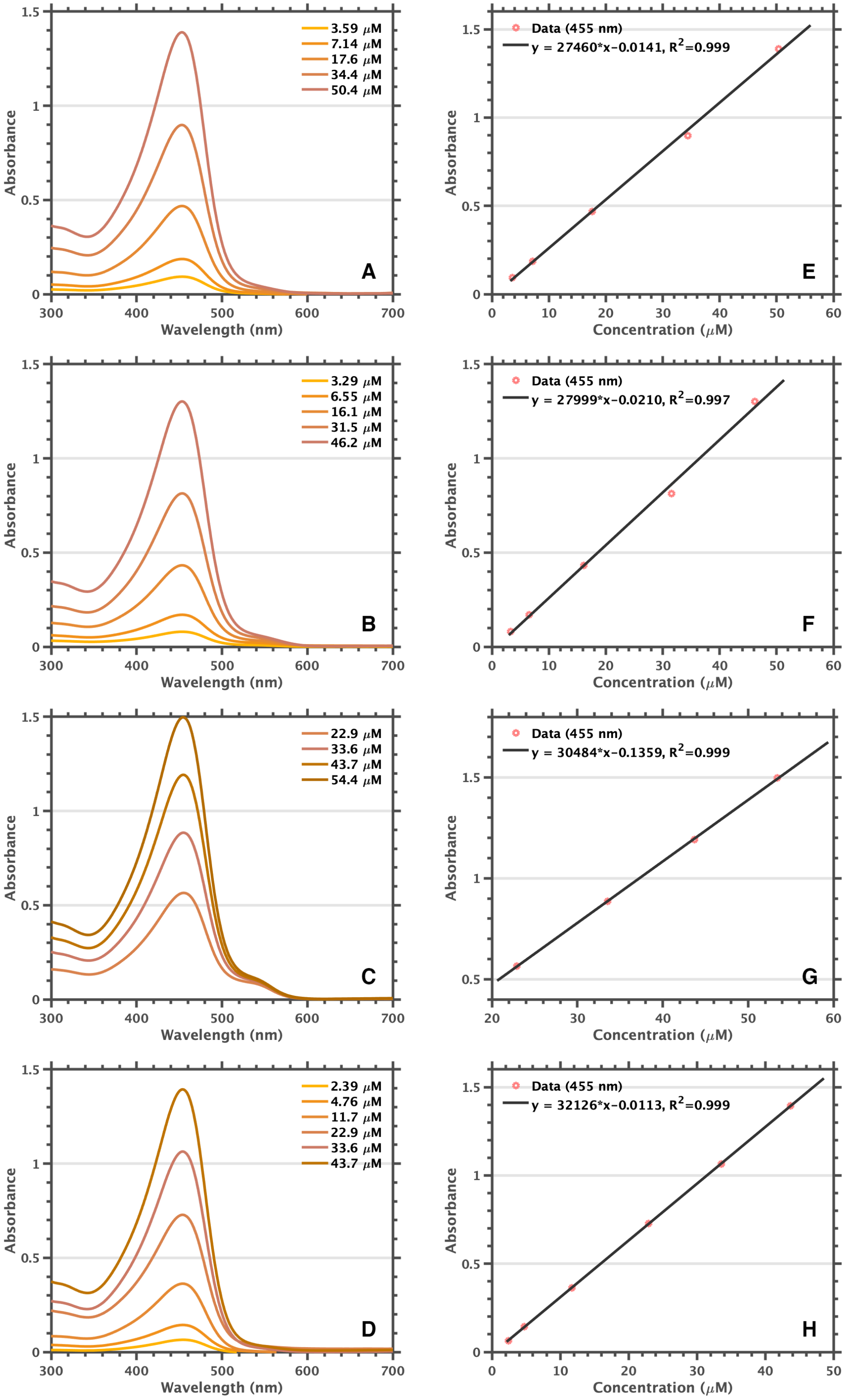

Figure 2.7. Beers' law study of $\mathbf{F_{60}}^0$ in (A, E) benzene, (B, F) toluene, (C, G) 1,2-dichlorobenzene and (D, H) chlorobenzene.

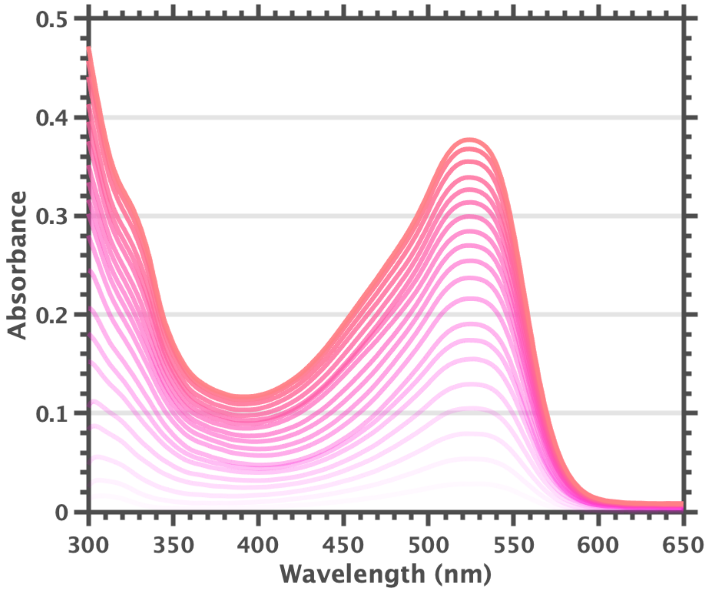

Figure 2.8. $\mathbf{F}_{60}{}^{0}$ in dry and degassed 1,2-dichlorobenzene. Slow addition of a concentrated solution to neat solvent. The 525 nm band indicates formation of $[\mathbf{F}_{60}]^{1-}$.

1,2-diiodo-tetrafluorobenzene to $\mathbf{F}_{60}{}^{0}$ and $\mathbf{F}_{84}{}^{0}$ samples prepared in 1,2-difluorobenzene. Spectra collect with and without 1,2-diiodo-tetrafluorobenzene are shown in Figure 2.9 (A-B). For $\mathbf{F}_{60}{}^{0}$ only a small 525 nm shoulder is present in neat 1,2-difluorobenzene. Addition of 1 mM 1,2-diiodo-tetrafluorobenzene leads to partial conversion to $[\mathbf{F}_{60}]^{1-}$. Increasing the 1,2-diiodo-tetrafluorobenzene concentration to 100 mM makes the effect more pronounced. $\mathbf{F}_{84}{}^{0}$ samples show a prominent 525 nm band even in neat 1,2-difluorobenzene and addition of a speck of 1,2-diiodo-tetrafluorobenzene leads to complete conversion to $[\mathbf{F}_{84}]^{1-}$.

Encouraged by these results we moved on to hexafluorobenzene, hoping to see a similar effect. Indeed, addition of a small amount of hexafluorobenzene caused bright yellow solutions of $\mathbf{F}_{60}{}^{0}$

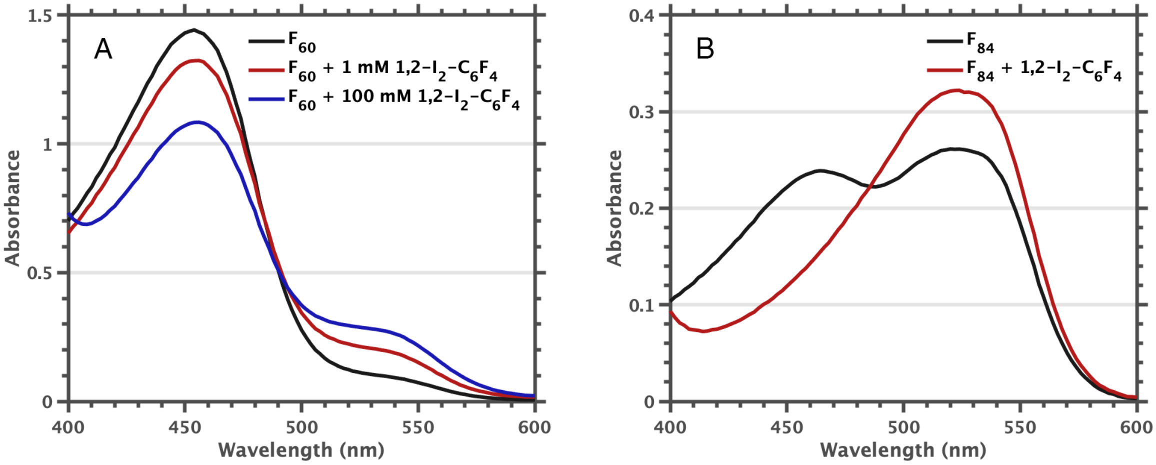

Figure 2.9 Addition of 1,2-diiodotetrafluorobezene to (A) $\mathbf{F_{60}}^0$ in 1,2-difluorobenzene and (B) $\mathbf{F_{84}}^0$ in 1,2-difluorobenzene.

to rapidly turn pink, indicating conversion to $[\mathbf{F_{60}}]^{1-}$. Figure 2.10 shows UV-visible spectra collected while titrating a chlorobenzene solution of $\mathbf{F_{60}}^0$ with hexafluorobenzene. At low hexafluorobenzene concentrations < 0.9 vol % (~80 mM) the absorption bands rapidly stabilize after each addition. However, conversion proceeds slowly at > 2 vol% (~170 mM) under low-light conditions, although rapid conversion can be achieved by illuminating the sample. Figure 2.11 shows the time-evolution of the absorption spectra after a rapid concentration increase from 0.9 vol% (~80 mM) to 2.2 vol% (~190 mM) hexafluorobenzene. The sample was kept in the dark between measurements and intermittent control spectra were taken to assure that the light absorbed during data collection did not significantly impact the spectrum.

The visible spectrum of $\mathbf{F_{60}}^0$ and $\mathbf{F_{84}}^0$ are very similar, displaying absorption maxima around 455 nm. However, a 525 nm shoulder is generally present in samples prepared in halogenated aromatic solvents. No evidence of aggregation-induced spectroscopic shifts are observed in the

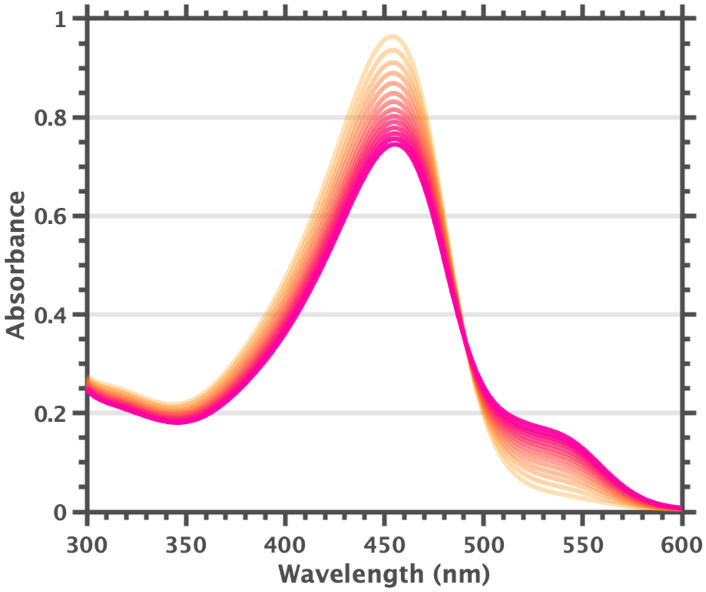

Figure 2.10. **F$_{60}$**^{0} in chlorobenzene. Titration with 0 – 0.9 vol% hexafluorobenzene.

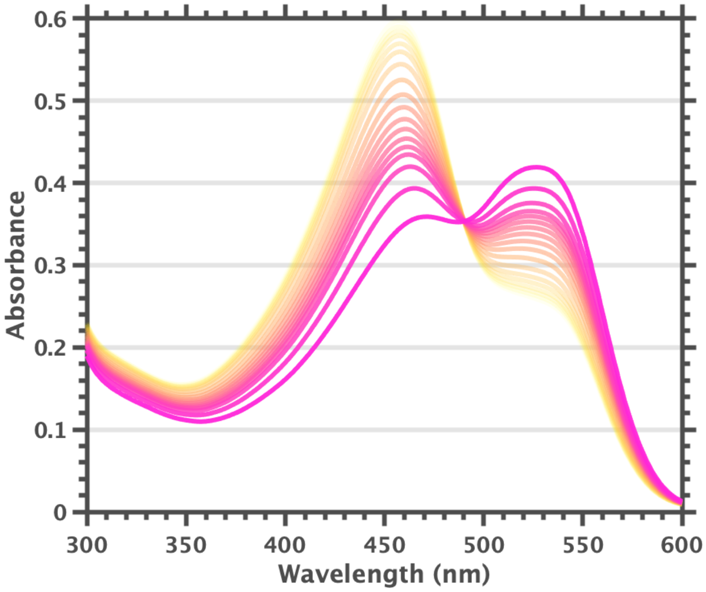

Figure 2.11. **F$_{60}$** in chlorobenzene. Time-evolution after increasing the hexafluorobenzene concentration from 0.9 vol% (~80 mM) to 2.2 vol% (~190 mM). Data points 1, 2, 3, 5, 7, 10, 15, 20, 25, 30, 35, 40, 45, 50, 60, 80 and 110 minutes after hexafluorobenzene addition.

Beer's Law studies, as expected assuming the 525 nm band stems from $[B_{12}]^{1-}$. However, the strong 525 nm band and near-complete 455 nm bleach resulting from slowly increasing the $\mathbf{F_{60}}^0$ concentration in 1,2-dichlorobenzene could signify that B_{12}^0 in high-concentration solutions exists in a kinetically inert aggregated form. More halogenated haloarenes result in a higher degree of conversion to the $[B_{12}]^{1-}$ state (hexafluorobenzene ≈ 1,2-diiodo-tetrafluorobenzene > 1,2-difluorobenzene > 1,2-dichlorobenzene > chlorobenzene); no 525 nm shoulder is observed under low-light conditions for $\mathbf{F_{60}}^0$ in chlorobenzene, while solutions containing a few vol% hexafluorobenzene show a strong 525 nm band and a near-complete bleaching of the 455 nm band (at equilibrium). The effect is further enhanced for $\mathbf{F_{84}}^0$. These observations indicate that interactions between the clusters and haloarenes result in a new species displaying the 525 nm band, presumably $[B_{12}]^{1-}$. Non-covalent interactions involving halogenated arenas are well known.[17–19] π-π stacking may occur between the haloarene and the aromatic rings on the clusters, which could induce conformational changes, redistribution of energy levels or formation of charge-transfer complexes. We propose that such interaction may result in modulation of the ring and haloarene molecular orbitals, possibly forming a combined ring-arene orbital. These modulated and/or combined molecular orbitals could act as donor orbitals resulting in $[\mathbf{F_{60}}]^{1-}$-$[\text{haloarene}]^{1+}$ charge-transfer complexes. TD-DFT calculations performed by collaborators in the Král group show that such interactions may a play role in styrene polymerization (see Appendix A). The data we have so far supports this description, however, it remains speculative and requires further experimental validation.

2.5 $[\mathbf{F_{60}}]^{1-}$ Disproportionation

Addition of triethylamine to solutions of $\mathbf{F_{60}}^0$ results in rapid conversion to $[\mathbf{F_{60}}]^{1-}$ (high triethylamine concentration leads to reduction to colorless $[\mathbf{F_{60}}]^{2-}$). Titration with strong acids, like trifluoroacetic acid or trifluoromethanesulfonic acid, on the other hand, restores the 455 nm and completely bleaches the 525 nm band. In fact, reversible bleaching and in-growth of the 455 nm and 525 nm bands can be achieved by addition of base followed by addition of acid, or vice versa. Figure 2.12 shows a trifluoroacetic acid titration of a 2 ml 2.5 μM $\mathbf{F_{60}}^0$ solution in 1,2-dichlorobenzene. The sample had been prepared by slow addition of a concentrated stock solution, so that the spectrum was dominated by $[\mathbf{F_{60}}]^{1-}$ (*vide supra*). 500 μl of a 1 vol% trifluoroacetic acid in 1,2-dichlorobenzene solution was added in 25 μl increments, resulting in samples containing between 0 and 26 mM trifluoroacetic acid. At 26 mM trifluoroacetic acid a small 525 nm shoulder is observed along with a strong 455 nm band. Addition of a 1% solution of triethylamine in 1,2-dichlorobenzene (225 μl in 25 μl increments) fully restores the 525 nm band, indicating complete recovery of $[\mathbf{F_{60}}]^{1-}$ at approximately 60 mM triethylamine (Figure 2.13).

It is notable that the magnitude of the 455 nm band at 26 mM trifluoroacetic acid is approximately the same as the magnitude of the 525 nm band of the starting solution. 1:1 conversion between $[\mathbf{F_{60}}]^{1-}$ and $\mathbf{F_{60}}^0$ should result in a 455 nm band of approximately twice the magnitude, given that $\varepsilon_{455\text{nm}}(\mathbf{F_{60}}^0)/\varepsilon_{525\text{nm}}([\mathbf{F_{60}}]^{1-}) \approx 2$ (see Section 2.2). These results indicate that only about half of $[\mathbf{F_{60}}]^{1-}$ is converted into $\mathbf{F_{60}}^0$, which suggest acid-induced disproportion into $\mathbf{F_{60}}^0$ and colorless $[\mathbf{F_{60}}]^{2-}$ (eq. 2.1).

$$[\boldsymbol{F_{60}}]^{1-} \rightleftharpoons {}^{1}\!/_{2}\, \boldsymbol{F_{60}}^{0} + {}^{1}\!/_{2}\, [\boldsymbol{F_{60}}]^{2-} \tag{2.1}$$

To understand this reactivity, we have to consider that triethylamine can act both as a weak reductant and as a weak base. Alone triethylamine acts as a reductant, reducing $\mathbf{F_{60}}^0$ to $[\mathbf{F_{60}}]^{1-}$. However, if triethylamine is added to the solution after acid-induced disproportionation, it

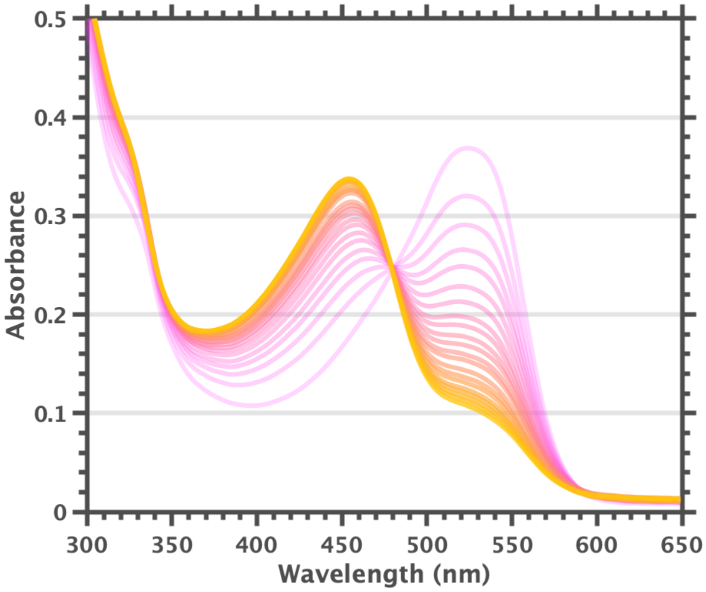

Figure 2.12. Titration of 2.5 μM [**F**$_{60}$]$^{1-}$ with trifluoroacetic acid. Each data point corresponds to addition of 25 μl 1% trifluoroacetic acid in 1,2-dichlorobenzene.

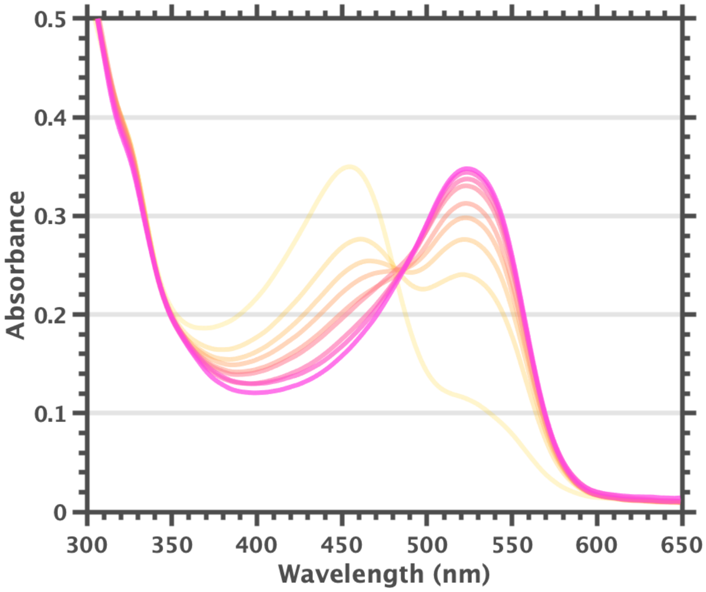

Figure 2.13. Recovery of [**F**$_{60}$]$^{1-}$ by addition of triethylamine. Each data point corresponds to addition of 25 μl 1% triethylamine in 1,2-dichlorobenzene.

instead acts as a base and reverses the disproportionation, either by decreasing the acidity or the ion strength of the solution. If $\mathbf{F_{60}}^0$ had instead been reduced by triethylamine, it would be apparent from following acid addition experiments, as multiple disproportionation-reduction cycles would result in accumulation of $[\mathbf{F_{60}}]^{2-}$ and lead to decoloration of the solution.

Variable temperature UV-visible studies in 2-methyltetrahydrofuran (2-MeTHF) show similar reversible color shifts. The room-temperature UV-visible spectrum of equilibrated 2-MeTHF solutions of $\mathbf{F_{60}}^0$ imply complete conversion to $[\mathbf{F_{60}}]^{1-}$. The conversion proceeds in the absence of light but is significantly faster under illumination. Intriguingly, visual observations suggest that cooling to 77 K (in 2-MeTHF glass) results in reoxidation to $\mathbf{F_{60}}^0$. In fact, the solution reversibly shifts color from deep purple at room temperature to bright yellow at 77 K. This behavior can be repeated over many freeze-thaw cycles. However, samples exposed to ambient lighting become paler over extended periods (hours) and remain purple at 77 K. A photograph displaying the prominent color shift observed upon freezing a fresh 2-MeTHF solution of $\mathbf{F_{60}}^0$ in liquid nitrogen is shown in Figure 2.11. Variable temperature UV-visible spectra (Figure 2.12) of $\mathbf{F_{60}}^0$ collected from 0ºC to -130ºC display a small 455 nm shoulder in the $\leq$ -100ºC range, suggesting that the yellow color stems from the 455 nm band. However, we are at this time unable to reach sufficiently low temperatures to clearly resolve the 455 nm band. (It is worth nothing that we observe vibrionic progression in the 525 nm band at cryogenic temperatures, with a spacing of ~500 cm^{-1}. This approximately matches the energy of B_{12}-core Raman breathing modes.[20]) Based on these observation, we hypothesize that $\mathbf{F_{60}}^0$ in 2-MeTHF fully converts to $[\mathbf{F_{60}}]^{1-}$ through (photo)oxidation of solvent, and that cooling to cryogenic temperatures result in disproportionation, yielding a spectrum dominated by the $\mathbf{F_{60}}^0$ 455 nm band. Over extended periods in ambient lighting, $[\mathbf{F_{60}}]^{1-}$ is converted to $[\mathrm{F_{60}}]^{2-}$ through solvent photooxidation. The increased [$\mathbf{F}_{60}$]$^{2-}$ concentration shifts the equilibrium so that disproportionation is no longer favored at 77 K.

The low-temperature behavior of $\mathbf{F_{60}}^0$ in 2-MeTHF was further explored by variable temperature ^{11}B- and ^{19}F-NMR collected from +65°C to -120°C. Based on the UV-visible spectrum, we assume complete conversion to [$\mathbf{F_{60}}$]$^{1-}$ at room temperature. The ^{11}B-NMR spectrum is featureless over the entire temperature range, as expected for paramagnetic [$\mathbf{F_{60}}$]$^{1-}$ (Figure 2.13). In line with previous reports,[21] the ^{19}F-NMR spectrum at ≥ +20°C shows two sharp resonances (1F, -158 ppm; 2F -165 ppm) corresponding to the meta and para positions on the perfluorophenyl rings. Additionally, a broad resonance is observed at -140 ppm, possibly stemming from the ortho position. Curiously, the fluorine resonances show significant broadening at lower temperatures and are near indistinguishable at -120°C (Figure 2.14).

The acid-base titration data and variable temperature UV-visible spectra suggest a disproportionation mechanism. Conversely, the lack of resonances in the variable temperature ^{11}B-NMR spectra indicate that the cluster remains paramagnetic. Low temperature and altered ionic strength is known to induce dimerization and other aggregation behaviors in some aromatic systems, which could lead to redistribution of charge and disproportionation.[22–25] We hypothesize that such disproportionated dimers/aggregates might form in 2-MeTHF at cryogenic temperatures, and could contribute to the broadening of the ^{19}F-NMR signals. The silent ^{11}B-NMR spectrum might be misleading, as the $\mathbf{F_{60}}^0$ and [$\mathbf{F_{60}}$]$^{2-}$ resonances could be too faint to be observable over the probe background. This explanation is corroborated by UV-visible spectra collected around -100°C, which indicate a low degree of disproportionation at the low-temperature limit of the NMR study.

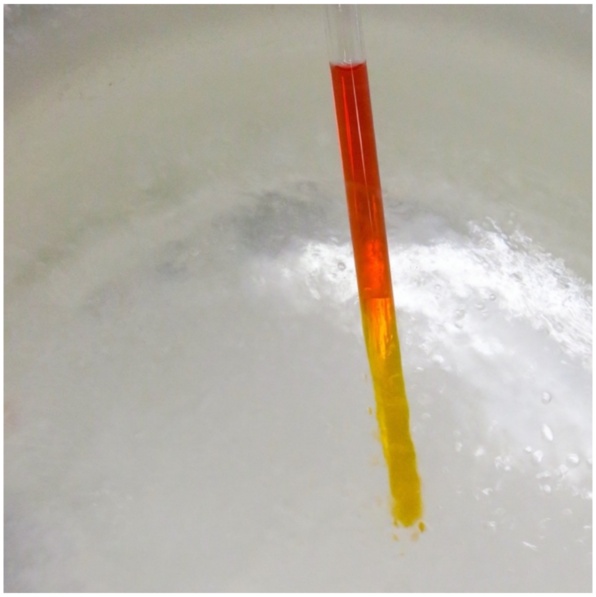

Figure 2.14. **F_{60}** in 2-MeTHF frozen in liquid nitrogen. The color shift is rapid and reversible.

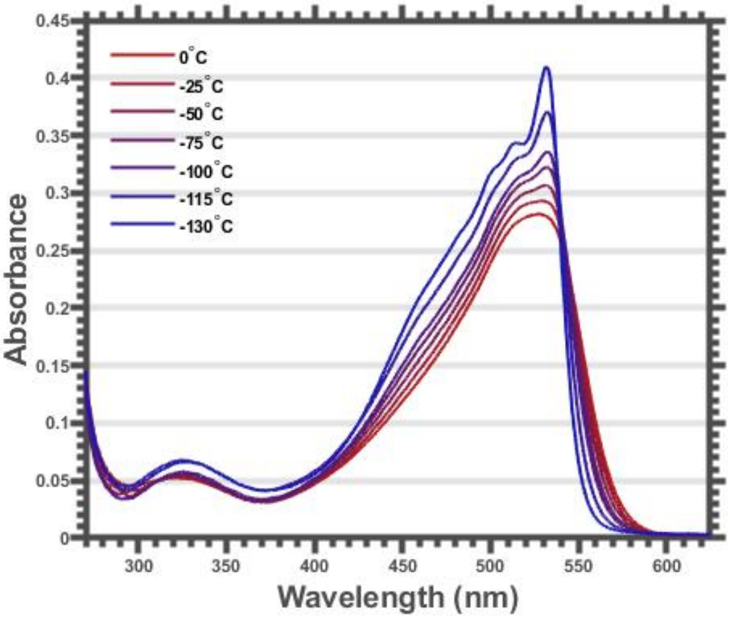

Figure 2.15. Variable temperature UV-visible spectra of **F_{60}** in 2-MeTHF collected from 0ºC to -130ºC. A 455 nm shoulder grows in at ≤ -100ºC.

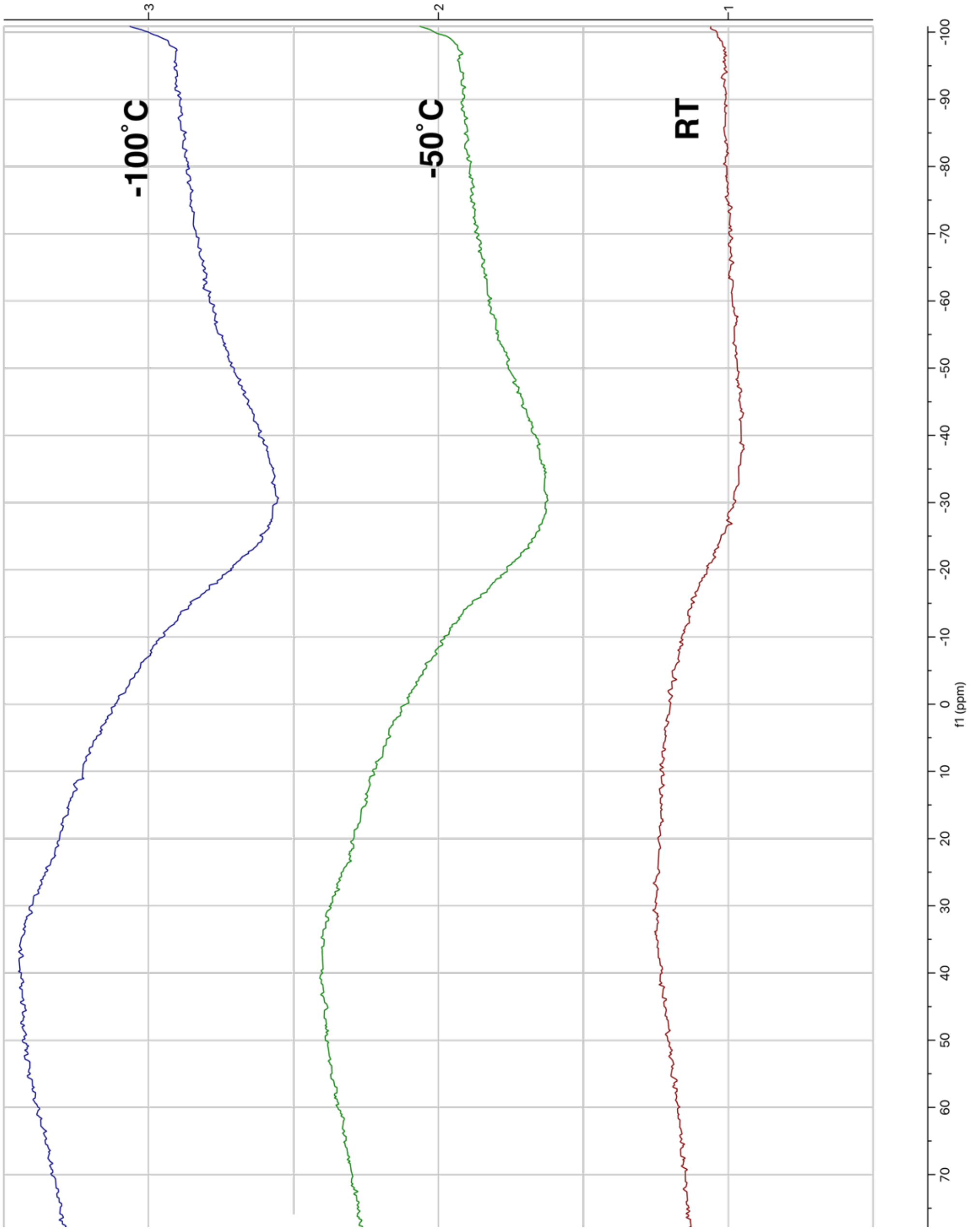

Figure 2.16. $\mathbf{F}_{60}^{0}$ in 2-MeTHF. ^{11}B-NMR collected at room temperature (red), -50°C (green) and -100°C (blue). Only the probe background signal is observed.

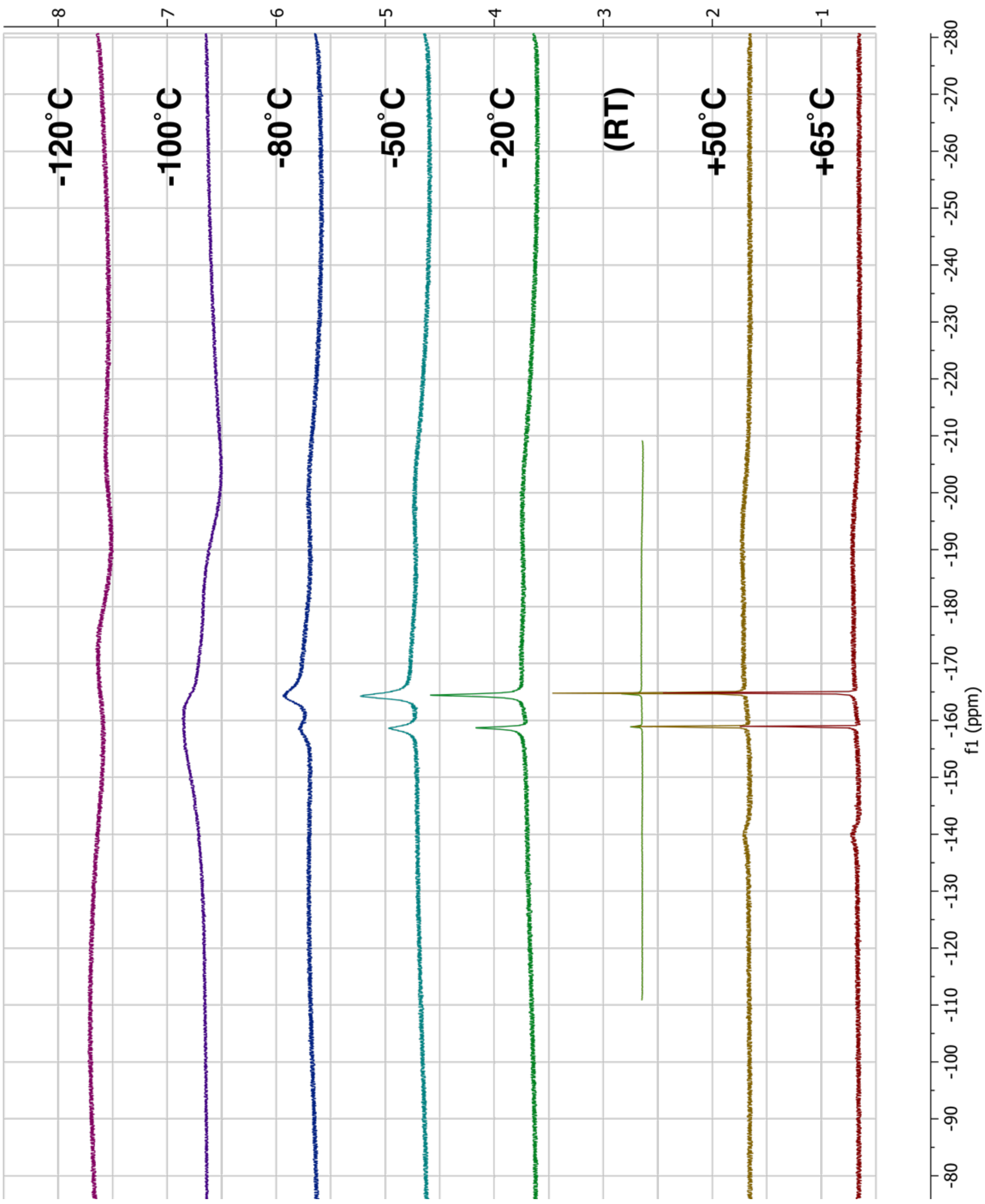

Figure 2.17. **F_{60}**^{0} in 2-MeTHF. Variable temperature ^{19}F-NMR spectra collected from +65°C to -120°C.

2.6 *hypercloso*-$B_{12}(OR)_{12}^0$ Emission

Although unable to definitively explain what causes the formation of the $[B_{12}]^{1-}$, we felt confident that obtaining reliable fluorescence spectra was dependent on preparation of samples containing only the 455 nm absorbing B_{12}^0 species. To determine optimal conditions, we explored two paths: (1) rigorous solvent purification and sample preparation and (2) exploration of alternative solvents. If formation of $[B_{12}]^{1-}$ by oxidation/photooxidation of impurities was the key issue, pure samples would be obtainable by sufficiently rigorous purification and sample preparation practices. However, if cluster-solvent interactions were involved, we would need to identify sufficiently non-interacting and oxidatively inert solvents.

We started by exploring the solvent purification path. Increasingly rigorous procedures were employed to prepare pure samples of $\mathbf{F_{60}^0}$ in benzene, toluene, 1,2-difluorobenzene and dichloromethane. Briefly, high-purity solvents were obtained (inhibitor free when relevant) and immediately dried over activated 3 Å molecular sieves for > 96 hours. After drying, solvents were distilled into Strauss flasks, discarding the initial and finals fractions. All manipulations were performed on a vacuum/argon manifold, with all glassware connected through glass joints. Ultra-high-purity argon, which was passed through oxygen and water scrubbers before entering the gas manifold, was used for all experiments. All glassware that came in contact with solution was cleaned in aqua regia before use. Following these procedures, no 525 nm shoulder was observed in the UV-visible spectra of $\mathbf{F_{60}}^0$ samples prepared under low-light conditions in dichloromethane, benzene and toluene. Upon prolonged and/or intense light-exposure, a minor 525 nm shoulder could be observed in both benzene and toluene. No fluorescence signal was observed above noise in any of these samples (450 nm excitation). UV-visible spectra of all $\mathbf{F_{60}}^0$ samples prepared in 1,2-difluorobenzene displayed a 525 nm shoulder, which grew when the sample was illuminated. Weak-to-medium intensity fluorescence, centered around 600 nm, was observed in these samples following 450 nm excitation. Further purification of 1,2-difluorobenzene, or use of solvents from different manufacturers, did not remove the 525 nm shoulder. These observations suggest that [$\mathbf{F_{60}}$]$^{1-}$ causes the 600 nm fluorescence. Solutions of $\mathbf{F_{60}}^0$ in 2-MeTHF, which appear to undergo complete conversion to [$\mathbf{F_{60}}$]$^{1-}$, provides further support of assigning the 600 nm fluorescence band to [$\mathbf{F_{60}}$]$^{1-}$. Figure 2.15 shows absorption, excitation and emission spectra of $\mathbf{F_{60}}$ in 2-MeTHF. The visible spectrum is identical to electrochemically generated [$\mathbf{F_{60}}$]$^{1-}$, and perfectly matched by the excitation spectrum.

As rigorous purification and sample preparation did not yield reliable fluorescence at room temperature, we started exploring alternative solvents. Dry and degassed octafluorotoluene was the only solvent were no formation of [$\mathbf{F_{60}}$]$^{1-}$ was observed at concentrations relevant for spectroscopy. Samples of $\mathbf{F_{60}}^0$ prepared in dry and degassed octafluorotoluene are stable for > 1 month under ambient lighting and show no spectral changes after prolonged laser illumination. Disappointingly, no fluorescence was observed for $\mathbf{F_{60}}^0$ solutions in octafluorotoluene at room temperature (450 nm excitation). We concluded that $\mathbf{F_{60}}^0$ does not display appreciable fluorescence at room temperature.

We turned our attention to low-temperature emission studies. Figure 2.16 shows emission spectra collected for $\mathbf{F_{60}}^0$ in toluene and 2-MeTHF glass at 77 K. In line with room-temperature data, $\mathbf{F_{60}}^0$ in toluene glass showed fluorescence centered around ~600 nm, likely stemming from trace [$\mathbf{F_{60}}$]$^{1-}$. In 2-MeTHF glass (freshly prepared), $\mathbf{F_{60}}^0$ displays low intensity fluorescence centered around 550 nm. This band could stem from $\mathbf{F_{60}}^0$, however, given the unusual temperature-dependent behavior of $\mathbf{F_{60}}^0$ in 2-MeTHF (Section 2.5) we felt these results did not provide a reliable representation of the neutral species. We decided to attempt 77 K studies of $[B_{12}]^0$ in octafluorotoluene. Neat octafluorotoluene does not glass well, but addition of ~10% perfluoro-methylcyclohexane results in clear glasses at 77 K. $\mathbf{F_{36}}^0$, $\mathbf{F_{60}}^0$ and $\mathbf{F_{72}}^0$ solutions in 10:1 octafluorotoluene/perfluoro-methylcyclohexane showed weak-to-medium intensity fluorescence at 77 K (Figure 2.17). $\mathbf{F_{36}}^0$ and $\mathbf{F_{72}}^0$ display bimodal emission, which we speculate could be due to the presence of two distinct conformations in solvent glasses. Dimerization mechanisms similar to what we suggested for $\mathbf{F_{60}}^0$ in 2-MeTHF (Section 2.5) may also be in play but seem less likely as the 77 K emission spectrum of $\mathbf{F_{60}}^0$ in 2-MeTHF is uncomplicated. Using the emission data at 77 K, we were able to calculate excited-state reduction potentials for $\mathbf{F_{36}}^0$ (~3.0 V), $\mathbf{F_{60}}^0$ (~ 3.2 V) and $\mathbf{F_{72}}^0$ (~ 3.3 V). Potentials are reported versus the standard calomel electrode (SCE).

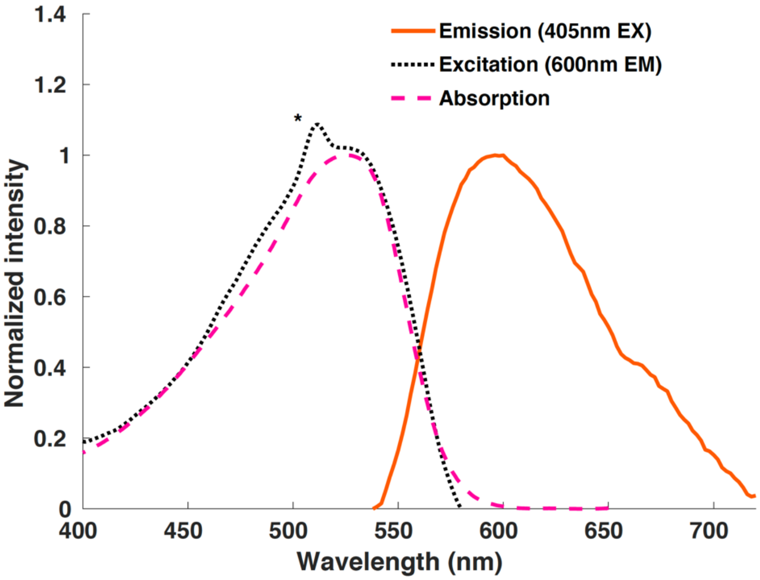

Figure 2.18. Absorption, excitation and emission spectra reported for $\mathbf{F_{60}}$ in 2-MeTHF. The excitation spectrum was collected monitoring 600 nm emission, while the emission spectrum was collected using 405 nm excitation.

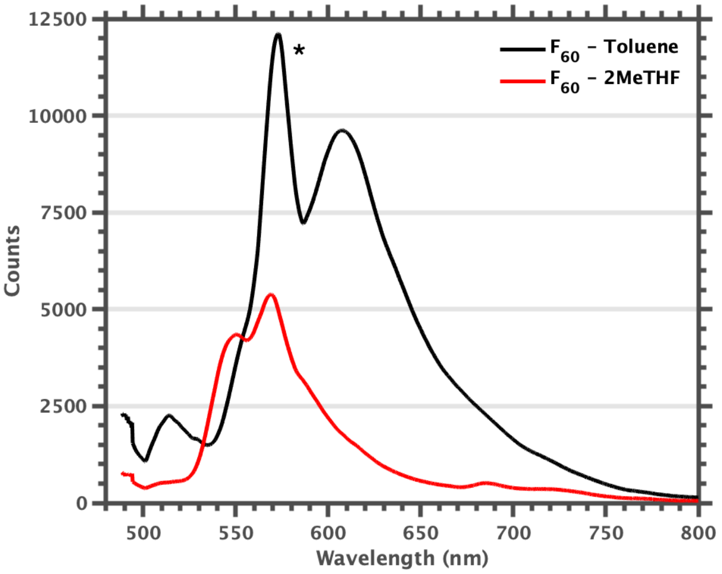

Figure 2.19. Emission spectrum of $\mathbf{F}_{60}^{0}$ in toluene and 2-MeTHF glass (77 K) excited at 457.9 nm. The peak denoted by * is caused by liquid nitrogen Raman scattering.

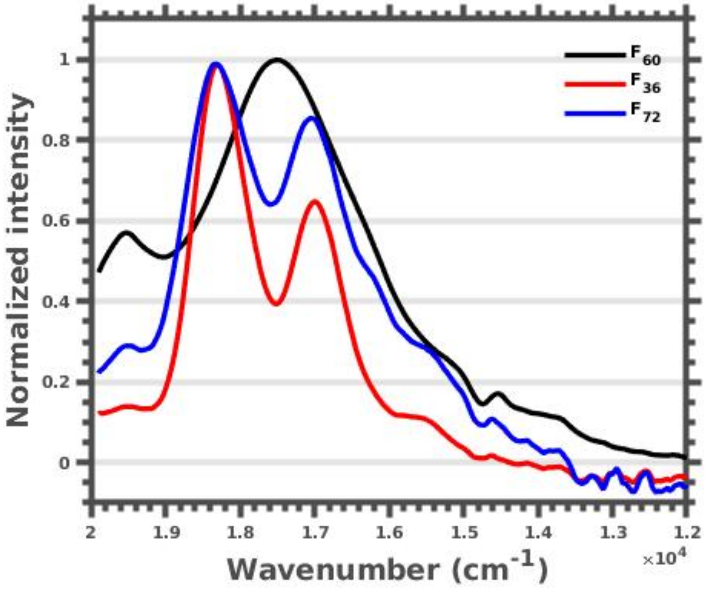

Figure 2.20. Emission spectra of $\mathbf{F}_{36}^{0}$, $\mathbf{F}_{60}^{0}$ and $\mathbf{F}_{72}^{0}$ in 10:1 octafluorotoluene/perfluoro-methylcyclohexane glass (77 K) excited at 457.9 nm.

2.7 Conclusions

Initial observations, reported in the Messina (2016) paper,[16] indicated that $[B_{12}]^0$ has lowest lying excited states with significant charge-transfer character and that the clusters exhibit complex emission stemming from multiple states. However, this was based on three assumptions that have later proved to be false (*vide supra*): (1) only the neutral clusters have strong ($> 10^4$ $M^{-1}cm^{-1}$) visible absorption bands, (2) the electronic transitions of interest must be of charge-transfer character to provide an excited state sufficiently long-lived to perform photochemistry in solution and (3) the clusters are relatively redox-stable in solution. The first assumption came from extinction coefficient measurements performed on isolated monoanionic $[B_{12}(OBz)_{12}]^{1-}$ and $[\mathbf{F_{60}}]^{1-}$ clusters. We now believe that the samples used for the reported extinction coefficient measurements were dominated the colorless dianionic species, which created the illusion of a relatively weak band 525 nm band. The true extinction coefficient of the 525 nm band is $> 10^4$ $M^{-1}cm^{-1}$. Viewing the 455 nm band as a charge-transfer transition makes sense considering the observed photochemistry, however, later work by us (see Chapter 4) has shown that this electronic transition is localized on the cluster core. Assumptions about the stability of the clusters in solution were based on that under the conditions used for photopolymerization reactions, which generally involved millimolar concentrations of the clusters, no noticeable color shifts occurred. At the much lower concentrations required for photophysical characterization illuminated samples quickly change from yellow to red-orange or purple due to cluster reduction.

Spectroelectrochemical data clearly shows that the 525 nm band belongs to $[\mathbf{F_{60}}]^{1-}$. It is our belief that the clusters participate in complex (photo)redox behaviors which explain most instances of $[\mathbf{F_{60}}]^{1-}$ formation. Under low-light conditions no 525 nm band is observed in the UV-visible spectrum of $\mathbf{F_{60}}^0$ in rigorously purified dichloromethane, benzene and toluene, suggesting that the 525 nm band seen in as-received solvents is primarily the result of spurious cluster reduction by impurities. However, after sufficient illumination the 525 nm band grows in even in samples prepared with rigorously purified solvents. These observations are readily explained by solvent photooxidation, consistent with the exceptionally high excited-state redox potential estimated for B_{12}^{0} clusters.

Although direct cluster reduction is a sufficient explanation under the conditions discussed above, interaction studies with haloarenes indicate that other mechanisms are also in play. Given the strong preference for $[\mathbf{F_{60}}]^{1-}$ in the presence of hexafluorobenzene and other highly halogenated arenes, it is likely that cluster-solvent interactions are involved. That said, it is possible that these observations are caused by impurities, although precautions have been taken to eliminate such contributions.

The room-temperature emission studies presented in this chapter indicate that the B_{12}^{0} excited state rapidly return to the ground state through non-radiative decay. Short lived excited states are not expected to substantially partake in solution based photoredox processes, as non-radiative decay outcompetes diffusion. However, electron transfer could proceed through a rapid tunneling mechanism if non-covalent cluster-monomer interactions occur in the ground state. The cluster-solvent interaction studies presented above, along with the computational work by Král and co-workers (Appendix A), support pre-association of clusters and monomers.

Although many question marks remain, the work presented here provided sufficient insight to guide us toward the computational and mechanistic studies presented in Appendix A. It would be interesting to further explore the intermolecular interactions and disproportionation mechanisms discussed in this chapter. However, we decided to, at least for the moment, leave these questions to the theoreticians. We felt our time was better spent exploring the electrochemical properties and electronic structure of $[B_{12}(OR)_{12}]$ clusters. That work is further discussed in Chapter 3 and 4.

2.8 Experimental Details

$B_{12}(OR)_{12}$ clusters

F_{36}, **F_{60}**, **F_{72}**, **F_{84}** were obtained from the Spokoyny lab and had been synthesized according to published procedures.[16,21]

UV-visible Spectroscopy

UV-visible spectra were collected on a Varian Cary 50 Bio spectrometer using a 1 cm path length quartz cuvettes, unless otherwise noted. All spectra were corrected by subtracting a solvent blank.

Electrochemistry

Sample preparation and electrochemical measurements were performed in an argon-filled glove box. Data was collected on a Gamry 600 Reference Potentiostat, using a small-volume electrochemical cell. Electrochemical grade $TBAPF_6$ (Sigma-Aldrich) had been previously recrystallized from hot ethanol and dried rigorously under vacuum. A d = 3.0 mm glassy carbon working electron (BASi), a Pt wire counter-electron and an Ag/AgCl reference electrode were used (BASi). The reference was prepared by placing a polished silver wire in a 0.01 M $AgNO_3$/0.2 M $TBAPF_6$ acetonitrile solution. A CoralPor (BASi) frit provided electrochemical contact between the reference solution and sample solution. Dichloromethane (Millipore) had been dried for > 84 hours over activated 3 Å molecular sieves (Sigma-Aldrich) and degassed through multiple freeze-pump-thaw cycles. Between each measurement the sample solution was thoroughly mixed, and the working electrode was polished with a Kimwipe (Kimtech) to remove any residue formed during preceding cycles. The EC-Lab software package (Biologic) was used to analyze the data.

Spectroelectrochemistry

The electrochemical setup was the same as described for the electrochemical experiments, with the exceptions noted below. Spectroelectrochemical data was collected on a Pine WaveNow potentiostat, using a 0.5 mm quartz spectroelectrochemistry (BASi) cell and gold mesh working electrode (BASi). Electrolytes were prepared at 0.1 M $TBAPF_6$. The experiments were conducted under ambient conditions. The electrolyte solution was degassed by argon bubbling.

In benzonitrile, the potential was held at +1.5 V to achieve full conversion to $\mathbf{F_{60}}^0$. The potential was the held at +0.2 V until $\mathbf{F_{60}}^0$ had been completely reduced to $[\mathbf{F_{60}}]^{1-}$. Finally, the potential was held at -0.5 V to reduce to $[\mathbf{F_{60}}]^{1-}$ to $[\mathbf{F_{60}}]^{2-}$. Complete conversion to $[\mathbf{F_{60}}]^{2-}$ was not achieved. In dichloromethane $\mathbf{F_{60}}^0$ was first reduced to $[\mathbf{F_{60}}]^{1-}$ by applying a -0.2 V bias (not shown). $[\mathbf{F_{60}}]^{2-}$ was generated by holding the potential at -0.5 V. $[\mathbf{F_{60}}]^{1-}$ was then fully recovered through applying a 0.85 V bias. Finally, $\mathbf{F_{60}}^0$ was regenerated by holding the potential at 2 V. Spectra were collected every 30 seconds.

Beer's Law Study

Toluene (Uvasol, Millipore), benzene (Uvasol, Millipore), chlorobenzene (Sigma-Aldrich) and dichlorobenzene (Sigma-Aldrich) were used as received. Stock solutions were prepared by dissolving $\mathbf{F_{60}}^0$ in toluene (3.6 mg, 0.72 mM), benzene (3.3 mg 0.66 mM), chlorobenzene (2.4 mg, 0.48 mM) and dichlorobenzene (2.4 mg 0.48 mM).

Aliquots of stock solution were added to achieve the desired $\mathbf{F_{60}}^0$ concentration. A flea stir bar was used to thoroughly mix the sample after each stock addition. The samples were given ample time to equilibrate.

Concentration Study

1,2-dichlorobenzene (Sigma-Aldrich) was dried over activated 3 Å molecular sieves for >48 hours before use. All manipulations were performed using standard air-free techniques.

A stock solution was prepared by dissolving 1.7 mg $\mathbf{F_{60}}^0$ in in 5 ml 1,2-dichlorobenzene. The solution was degassed by three 15 minute freeze-pump-thaw cycles. Neat solvent was separately freeze-pump-thawed over three 15 minute cycles, and 1.5 ml was transferred to septum sealed cuvette equipped with a flea stir bar. Stock solution was added 25 ul at a time using a gas-tight syringe. The sample was allowed to equilibrate under stirring after each addition. A spectrum was collected for each equilibrated solution.

Interaction with 1,2-Iodo-Tetrafluorobenzene

A stock solution of $\mathbf{F_{60}}^0$ in 1,2-difluorobenzene was prepared at approximately 50 μM concentration. A spectrum was collected of the neat $\mathbf{F_{60}}^0$ solution. Two 5 ml aliquots were taken aside for interaction experiments. ~2 mg (1 mM) 1,2-diiodo-tetrafluorobenzene was added to one of the 5 ml aliquots and ~200 mg (200 mM) 1,2-diiodotetrafluorobezene was added to the second 5 ml aliquot. The samples were given ample time to equilibrate. Final data were collected when the spectrum remained steady for several minutes.

A speck of $\mathbf{F_{84}}^0$ was added to a cuvette containing 3 ml 1,2-difluorobenzene. A spectrum was collected of the neat $\mathbf{F_{84}}^0$ solution. Then a small speck of 1,2-diiodo-tetrafluorobezene (< 1 mg) was added to the cuvette. After ample mixing and equilibration time a second spectrum was collected. Additional spectra were collected to assure that the sample had equilibrated.

Interaction with Hexafluorobenzene

A ~40 μM solution of $\mathbf{F_{60}}^{0}$ in chlorobenzene (Sigma-Aldrich) was transferred to a 1 cm path length quarts cuvette. Hexafluorobenzene (Sigma-Aldrich, NMR-grade) was added in 1 μl increments until a total of 18 μl had been added. Spectra were collected after each addition, first giving the sample ample time to equilibrate. A time-evolution series was collected by adding another 27 μl of hexafluorobenzene. Time points were collected until the spectrum stabilized.

Acid Titration

The initial solution was prepared by slow addition of a concentrated $\mathbf{F_{60}}^{0}$ solution to neat 1,2-dichlorobenzene, resulting in a sample dominated by $[\mathbf{F_{60}}]^{1-}$. A 1 vol% solution of trifluoroacetic acid was added to the sample in 25 μl increments until a total of 500 μl had been added. The sample was equilibrated under ambient lighting after each addition.

After completion of the acid titration, the sample was titrated with a 1 vol% solution of triethylamine in 1,2-dichlorobenzene, added in 25 μl increments until a total of 225 μl had been added. Unlike the acid titration steps, which required minutes of equilibration, the spectral changes upon triethylamine addition were near-instant. Attempts to add additional trifluoroacetic acid after the final data point resulted in formation of a white precipitate.

Variable Temperature Studies in 2-MeTHF

2-MeTHF (Sigma-Aldrich, anhydrous) was dried over activated 3 Å molecular sieves for > 48 hours and degassed through three 30 minute freeze-pump-thaw cycles. NMR samples were prepared in quartz J. Young tubes. A small speck of $\mathbf{F_{60}}^{0}$ was added to the tube and dried under vacuum for > 30 minutes, over three argon/vacuum cycles. Solvent was vacuum transferred to the J. Young tube. Complete conversion to $[\mathbf{F_{60}}]^{1-}$ was achieved by illuminating the sample with a 450 nm laser pointer (Roithner Lasertechnik). UV-visible samples were prepared in 1 cm path length screw-cap cuvettes inside a nitrogen-filled glovebox. Variable temperature NMR spectra were collected on a Varian 400 MHz Spectrometer with a broadband auto-tune OneProbe. A Varian Cary 50 UV-visible spectrometer equipped with a Unisoku CoolSpek cryostat was used to collect variable temperature UV-visible spectra. The samples were given ample time to equilibrate before each measurement. UV-visible spectra were corrected by subtracting solvent background spectra collect at each temperature point.

Visual observations were performed using X-band EPR tubes; no difference was observed between open-air and air-free samples. After preparation, the sample was illuminated using a 450 nm laser pointer to achieve complete conversion to $[\mathbf{F_{60}}]^{1-}$. The samples were submerged in liquid nitrogen to obtain a 2-MeTHF glass, resulting in an immediate color shift from deep purple to bright yellow. Thawing of the sample rapidly restored the color to deep purple.

Room-Temperature Emission

The following solvents were dried for > 96 hours and degassed though freeze-pump-thawing: toluene (Millipore), 2-MeTHF (Sigma-Aldrich), benzene (Millipore), chlorobenzene (Sigma-Aldrich), 1,2-difluorobenzene (Sigma-Aldrich), dichloromethane (Fischer., inhibitor free) and perfluorotoluene (TCI). Schlenk cuvettes with a separate compartment for sample preparation and degassing were used. All glassware was thoroughly oven-dried before use. Solid compounds were handled open-air but all steps following addition of solid to the sample compartment were performed using standard air-free techniques.

Under argon backflow a small amount of the cluster was added to the sample compartment. The solids were dried and degassed under vacuum. The solvent was vacuum transferred into the sample compartment, thawed and mixed to dissolve the solids. The sample solution was degassed by three 15 minute freeze-pump-thaw cycles, after which the solution was transfer to the cuvette compartment. Formation of $[B_{12}]^{1-}$ was assessed visually and by UV-visible spectroscopy.

Preliminary fluorescence spectra were collected on all samples, regardless of whether $[B_{12}]^{1-}$ was present or not. A FluoroLog Modular Spectrofluorometer (Horiba Jobin Yvon) was used to for photoluminescence measurements. Emitted light was passed through a monochromator and recorded by a PMT detector. Stronger 600 nm fluorescence was observed for samples containing more $[B_{12}]^{1-}$.

77 K Emission

Toluene (Millipore), 2-MeTHF (Sigma-Aldrich) and perfluorotoluene (TCI) and perfluoromethylcyclohexane (TCI) had been dried over 3 Å molecular sieves (> 48 hours) and degassed through at least three freeze-pump-thaw cycles. X-band quartz EPR tubes (ID = 3 mm, OD = 4 mm) were used to hold the samples. All glassware and cannulae had been thoroughly overdried before use. $\mathbf{F_{60}}$, $\mathbf{F_{72}}$, and $\mathbf{F_{84}}$ were handled open-air. All steps following addition of compound to the sample preparation vessel were performed under argon/vacuum using standard air-free techniques.

A small speck of compound was transferred to a 20 ml scintillation vial equipped with a septum cap. The solids were dried and degassed under vacuum for at least 30 minutes, minimum three argon/vacuum cycles. Solvent was added by cannula, the samples mixed and finally transferred to the EPR tube under argon backflow. The samples were immediately frozen in liquid nitrogen. A 457.9 nm excitation source (Coherent Innova 70) was used. Emitted light was directed to a

Melles Griot 13 FOS 200 Spectrometer through an optical fiber. A 457.9 nm long-pass cutoff filter was used to exclude excitation light. The reduction potentials of photo-excited $B_{12}{}^{0}$ clusters were approximated[26] using eq. 2.2,

$$E^{*}_{red}{}^{0} = E_{red}{}^{0} + E_{0,0} \tag{2.2}$$

where $E_{red}{}^{0}$ represents the ground-state 0/1- redox couple of and $E_{0,0}$ represents the wavelength of the onset of fluorescence. Redox values were calculated based on the Fc/Fc^{+} reference and converted to SCE, based on values reported by Connelly and Geiger,[27]. The potential of Fc/Fc^{+} referenced to SCE in CH_3CN with $TBAPF_6$ as the supporting electrolyte is 0.40 V.

BIBLIOGRAPHY

(1) Axtell, J. C.; Messina, M. S.; Liu, J.-Y.; Galaktionova, D.; Schwan, J.; Porter, T. M.; Savage, M. D.; Wixtrom, A. I.; Rheingold, A. L.; Kubiak, C. P.; et al. Photooxidative Generation of Dodecaborate-Based Weakly Coordinating Anions. *Inorg. Chem.* **2019**, *58* (16), 10516–10526. https://doi.org/10.1021/acs.inorgchem.9b00935.

(2) Lipscomb, W. N. Recent Studies of the Boron Hydrides. In *Advances in Inorganic Chemistry and Radiochemistry*; Emeléus, H. J., Sharpe, A. G., Eds.; Academic Press, 1959; Vol. 1, pp 117–156. https://doi.org/10.1016/S0065-2792(08)60253-8.

(3) Lipscomb, W. N.; Britton, D. Valence Structure of the Higher Borides. *J. Chem. Phys.* **1960**, *33* (1), 275–280. https://doi.org/10.1063/1.1731097.

(4) Eberhardt, W. H.; Crawford, B.; Lipscomb, W. N. The Valence Structure of the Boron Hydrides. *J. Chem. Phys.* **1954**, *22* (6), 989–1001. https://doi.org/10.1063/1.1740320.

(5) Hoffmann, R.; Lipscomb, W. N. Theory of Polyhedral Molecules. I. Physical Factorizations of the Secular Equation. *J. Chem. Phys.* **1962**, *36* (8), 2179–2189. https://doi.org/10.1063/1.1732849.

(6) Wunderlich, J. A.; Lipscomb, W. N. STRUCTURE OF B12H12-2 ION. *J. Am. Chem. Soc.* **1960**, *82* (16), 4427–4428. https://doi.org/10.1021/ja01501a076.

(7) Moore, E. B.; Lohr, L. L.; Lipscomb, W. N. Molecular Orbitals in Some Boron Compounds. *J. Chem. Phys.* **1961**, *35* (4), 1329–1334. https://doi.org/10.1063/1.1732046.

(8) Hoffmann, R.; Lipscomb, W. N. Boron Hydrides: LCAO—MO and Resonance Studies. *J. Chem. Phys.* **1962**, *37* (12), 2872–2883. https://doi.org/10.1063/1.1733113.

(9) Longuet-Higgins, H. C.; Roberts, M. D. V. The Electronic Structure of an Icosahedron of Boron Atoms. *Proc R Soc Lond A* **1955**, *230* (1180), 110–119. https://doi.org/10.1098/rspa.1955.0115.

(10) Peymann, T.; Knobler, C. B.; Hawthorne, M. F. An Unpaired Electron Incarcerated within an Icosahedral Borane Cage: Synthesis and Crystal Structure of the Blue, Air-Stable {[Closo-B12(CH3)12]·}– Radical. *Chem. Commun.* **1999**, *0* (20), 2039–2040. https://doi.org/10.1039/A905406E.

(11) Boeré, R. T.; Bolli, C.; Finze, M.; Himmelspach, A.; Knapp, C.; Roemmele, T. L. Quantum-Chemical and Electrochemical Investigation of the Electrochemical Windows of Halogenated Carborate Anions. *Chem. – Eur. J.* **2013**, *19* (5), 1784–1795. https://doi.org/10.1002/chem.201202475.

(12) Boeré, R. T.; Derendorf, J.; Jenne, C.; Kacprzak, S.; Keßler, M.; Riebau, R.; Riedel, S.; Roemmele, T. L.; Rühle, M.; Scherer, H.; et al. On the Oxidation of the Three-Dimensional Aromatics [B12X12]2− (X=F, Cl, Br, I). *Chem. – Eur. J.* **2014**, *20* (15), 4447–4459. https://doi.org/10.1002/chem.201304405.

(13) Boeré, R. T.; Kacprzak, S.; Keßler, M.; Knapp, C.; Riebau, R.; Riedel, S.; Roemmele, T. L.; Rühle, M.; Scherer, H.; Weber, S. Oxidation of Closo-[B12Cl12]2− to the Radical Anion [B12Cl12].− and to Neutral B12Cl12. *Angew. Chem. Int. Ed.* **2011**, *50* (2), 549–552. https://doi.org/10.1002/anie.201004755.

(14) Van, N.; Tiritiris, I.; Winter, R. F.; Sarkar, B.; Singh, P.; Duboc, C.; Muñoz-Castro, A.; Arratia-Pérez, R.; Kaim, W.; Schleid, T. Oxidative Perhydroxylation of [Closo-B12H12]2− to the Stable Inorganic Cluster Redox System [B12(OH)12]2−/.−: Experiment and Theory. *Chem. – Eur. J.* **2010**, *16* (37), 11242–11245. https://doi.org/10.1002/chem.201001374.

(15) Peymann, T.; Knobler, C. B.; Khan, S. I.; Hawthorne, M. F. Dodeca(Benzyloxy)Dodecaborane, B12(OCH2Ph)12: A Stable Derivative of Hypercloso-B12H12. *Angew. Chem. Int. Ed.* **2001**, *40* (9), 1664–1667. https://doi.org/10.1002/1521-3773(20010504)40:9<1664::AID-ANIE16640>3.0.CO;2-O.

(16) Messina, M. S.; Axtell, J. C.; Wang, Y.; Chong, P.; Wixtrom, A. I.; Kirlikovali, K. O.; Upton, B. M.; Hunter, B. M.; Shafaat, O. S.; Khan, S. I.; et al. Visible-Light-Induced Olefin Activation Using 3D Aromatic Boron-Rich Cluster Photooxidants. *J. Am. Chem. Soc.* **2016**, *138* (22), 6952–6955. https://doi.org/10.1021/jacs.6b03568.

(17) Williams, J. H.; Cockcroft, J. K.; Fitch, A. N. Structure of the Lowest Temperature Phase of the Solid Benzene–Hexafluorobenzene Adduct. *Angew. Chem. Int. Ed. Engl.* **1992**, *31* (12), 1655–1657. https://doi.org/10.1002/anie.199216551.

(18) Grimme, S. Do Special Noncovalent π–π Stacking Interactions Really Exist? *Angew. Chem. Int. Ed.* **2008**, *47* (18), 3430–3434. https://doi.org/10.1002/anie.200705157.

(19) Martinez, C. R.; Iverson, B. L. Rethinking the Term “Pi-Stacking.” *Chem. Sci.* **2012**, *3* (7), 2191–2201. https://doi.org/10.1039/C2SC20045G.

(20) Muetterties, E. L.; Merrifield, R. E.; Miller, H. C.; Knoth, W. H.; Downing, J. R. Chemistry of Boranes. III.1 The Infrared and Raman Spectra of B12H12 - and Related Anions. *J. Am. Chem. Soc.* **1962**, *84* (13), 2506–2508. https://doi.org/10.1021/ja00872a011.

(21) Wixtrom, A. I.; Shao, Y.; Jung, D.; Machan, C. W.; Kevork, S. N.; Qian, E. A.; Axtell, J. C.; Khan, S. I.; Kubiak, C. P.; Spokoyny, A. M. Rapid Synthesis of Redox-Active Dodecaborane B12(OR)12 Clusters under Ambient Conditions. *Inorg. Chem. Front.* **2016**, *3* (5), 711–717. https://doi.org/10.1039/C5QI00263J.

(22) De Sorgo, M.; Wasserman, B.; Szwarc, M. Aggregation of Salts of Thianthrene Radical Cations. *J. Phys. Chem.* **1972**, *76* (23), 3468–3471. https://doi.org/10.1021/j100667a029.

(23) Penneau, J. F.; Stallman, B. J.; Kasai, P. H.; Miller, L. L. An Imide Anion Radical That Dimerizes and Assembles into .Pi.-Stacks in Solution. *Chem. Mater.* **1991**, *3* (5), 791–796. https://doi.org/10.1021/cm00017a013.

(24) Rapta, P.; Dunsch, L. Dimerisation of Organic Radical Ions and Redox Reactions of Dimers as Studied by Temperature-Dependent in Situ ESR/UV–Vis–NIR Spectroelectrochemistry. *J. Electroanal. Chem.* **2001**, *507* (1), 287–292. https://doi.org/10.1016/S0022-0728(01)00473-9.

(25) Nishinaga, T.; Komatsu, K. Persistent π Radical Cations: Self-Association and Its Steric Control in the Condensed Phase. *Org. Biomol. Chem.* **2005**, *3* (4), 561–569. https://doi.org/10.1039/B418872A.

(26) Gray, H. B.; Maverick, A. W. Solar Chemistry of Metal Complexes. *Science* **1981**, *214* (4526), 1201–1205. https://doi.org/10.1126/science.214.4526.1201.

(27) Connelly, N. G.; Geiger, W. E. Chemical Redox Agents for Organometallic Chemistry. *Chem. Rev.* **1996**, *96* (2), 877–910. https://doi.org/10.1021/cr940053x.